anti-HBsAg microbeads (Abott) by incubation overnight at 4°C. The beads were then washed three times in PBS followed by centrifugation for 30 sec at 4°C. Then the beads were suspended in Laemmli buffer containing β-mercaptoethanol, boiled for 5 min at 95°C, and subjected to SDS-PAGE and Western blot with anti-human IgG Fc antibody. As the quantitative control of Western blot, 125, 250 and 500 ng of EC-Fc was applied at the same time. Thus, the efficient ratio of EC-Fc and ZZ-BNC was determined and the multivalent form of EC-1 peptide was prepared as EC-Fc/BNC. BNC bound to Fc protein (Fc/BNC) was prepared simultaneously as a control.

Confocal microscopic observation of ErbB2 internalization

For confocal microscopic observation, cells were grown on 35 mm glass base dish (Iwaki Science Products, Japan). With the conditioned media prepared from CHO cells expressing EC-Fc or Fc proteins in HEPES buffered RPMI-1640 supplemented with 1% BSA, the target cells were incubated for 90 min at 37°C. The cells were fixed with 4% paraformaldehyde in PBS, permeabilized with 0.2% Triton X-100 and were blocked with 1% BSA or 10% FBS in PBS. Then the cells were washed with PBS and incubated with FITC-labelled anti-human IgG Fc antibody (Sigma-Aldrich) diluted 1:500 for 30 min at 37°C. Prior to the preparation of EC-Fc/BNC or Fc/BNC, BNC was labelled with RITC (Sigma-Aldrich). Cells were incubated with RITC-labelled EC-Fc/BNC or Fc/BNC for 1, 4 and 8 hrs. The cells were washed with PBS and were fixed with 4% paraformaldehyde in PBS and then permeabilized with 0.1% TritonX-100 for 5 min. The fixed and permeabilized cells were blocked with 1% BSA in PBS and incubated with anti-ErbB2 antibody sc-08 (Santa Cruz Biotechnology, CA) for 1 hr followed by Alexa 488–labelled anti-rabbit IgG (Molecular Probe Inc., OR) for 30 min. After washing the cells with PBS, the visualization were carried under a confocal microscope, LSM 510 Meta (Carl Zeiss, Germany) equipped with Argon laser and LSM software (Carl Zeiss, Germany). Argon laser with excitation laser line of 488 nm coupled with the band-pass filter of 505 nm was used for the fluorescence of FITC and Alexa 488. He–Ne with 543 nm laser line coupled with the band-pass filter of 560 nm for the fluorescence of RITC. For inhibition studies, Chlorpromzine (CPZ; Wako Pure-Chemicals, Japan) and Methyl β-cyclodextrin (mβCD) was procured from Sigma Aldrich. The percentage of colocalization was calculated from Manders' overlapping coefficients (red overlapping green) using the JACoP plugin of ImageJ.

Biotinylation assay for the internalization of ErbB2

Biotinylation was performed as described previously [24]. Briefly, 5×10^5 cells were plated and cultured in a 60-mm tissue culture dish with complete medium. At the 90% confluency, the cells were washed twice in Hanks' balanced salt solution (HBSS) for 10 min at 4°C. Sulfo-NHS-SS-Biotin (Pierce Chemical) dissolved in HBSS at a concentration of 0.5 mg/ml was added to the cells at 4°C with mild shaking for 20 min. This reaction was repeated twice. The cells were washed with HEPES buffered RPMI supplemented with 1% BSA and 2 mM glutamine (RPMI-BSA) for 10 min at 4°C. Cells were incubated with either 30 μg/ml EC-Fc protein, or anti-ErbB2 monoclonal antibody sc-08 diluted to 1:100 in RPMI-BSA for 1 hr at 37°C. For the multivalent display studies the SK-BR-3 cells were incubated with 20, 100 and 200 nM of EC-Fc and 1, 5 and 10 nM of EC-Fc/BNC, where EC-Fc:BNC = 20:1. The cells incubated with anti-ErbB2 antibody sc-08 were washed and incubated for 1 hr at 37°C with HRP conjugated anti-mouse IgG (Cell Signaling Technology, MA) diluted to 1:400 with RPMI-BSA. The incubation was stopped by transferring the dishes back on ice, and the cells rinsed twice with HBSS. The biotin on the cell surface was cleaved under reducing condition of 20 mM DTT in 50 mM Tris-HCl, pH 8.7 containing 100 mM NaCl and 2.5 mM $CaCl_2$ for 20 min at 4°C, which was repeated twice. The cells were then washed three times with HBSS, and lysed in the lysis buffer consisting of 50 mM Tris-HCl, pH 7.4, 150 mM NaCl, 2 mM EDTA, 1% Triton X-100, 10 mM NaF, 1 mM vanadate, and protease inhibitor cocktail (Sigma-Aldrich) by the incubation for 20 min at 4°C. The lysates were collected and sonicated twice, and cell extracts were clarified by centrifugation for 5 min at 4°C. Protein concentrations in the extracts were determined by BCA assay (Pierce Chemical). Twenty microlitres of avidin agarose (Sigma-Aldrich) was added to the extracts and incubated overnight at 4°C. After centrifugations for 30 sec at 4°C, the agarose was washed three times in the lysis buffer, suspended in Laemmli buffer supplemented with β-mercaptoethanol, heated 5 min at 95°C, and subjected to SDS-PAGE followed by Western blotting. Transferrin receptor internalization was taken as a control for the immunoprecipitation experiments because transferrin is constitutively replenished from the surface of the cell to the endosome and from recycling endosome to the cell surface.

Analysis of cellular uptake of EC-Fc/BNC

The receptor-mediated cellular uptake of EC-Fc/BNC was evaluated. The cells in 60-mm dish were washed twice with ice-cold PBS and incubated with 2 nM (10 μg/ml) of EC-Fc/BNC for 5 hrs at 4°C or 37°C. After incubation, the cells were washed twice with ice-cold PBS to remove unbound BNC and then collected by the treatment with 0.025% trypsin. After centrifugation at 6,000 rpm for 1 min the supernatant was discarded and the cell pellet was washed twice with ice-cold PBS. The cells were then lysed in the lysis buffer, further incubated for 20 min at 4°C and sonicated twice. The cell extracts were clarified by centrifugation for 5 min at 4°C. Twenty microlitres of anti-HBsAg microbeads suspension was added to the extracts and incubated overnight at 4°C. After centrifugations for 30 sec at 4°C, the beads were washed three times in PBS, suspended in Laemmli buffer supplemented with β-mercaptoethanol, heated for 5 min at 95°C, and subjected to SDS-PAGE followed by Western blotting.

Flow cytometric analysis of ErbB2 internalization

For flow cytometric analysis, the cells seeded in a 100-mm dish were washed with PBS and were collected with enzyme free cell dissociation buffer (GIBCO) after incubating at 37°C for 5 min. The dissociation reaction was stopped by adding serum to the sample. Five hundred thousand cells were suspended in 0.1% BSA, containing 0.1% sodium azide in PBS (PBSB). After suspended in PBSB supplemented with EC-Fc, EC-Fc/BNC, Fc and Fc/BNC the cells were subsequently incubated on ice for 30 min. For internalization experiment, the cells were fixed and then permeabilized with 0.2% Triton X-100 in PBS. Then washed with PBSB, the cells were incubated with anti-human Fc antibody labelled with FITC at a dilution of 1:500 in PBSB followed by incubation on ice for 30 min. The cells were then processed for flow cytometric analysis by a FACS Calibur (Becton, Dickinson and Company).

Western blotting and image analysis

Proteins resolved on acrylamide gel were transferred to a polyvinylidene difluoride (PVDF) membrane (Bio-Rad, VA). The membrane was blocked

with 10% skim milk in 10 mM Tris-HCl, pH 7.4, 150 mM NaCl containing 0.1% Tween-20 (TBST). The blots were then probed with a biotinylated polyclonal anti-human IgG antibody diluted to 1:1,000 (Dako, Denmark) or anti–preS-1 monoclonal antibody (Beacle, Japan) conjugated to HRP diluted to 1:15,000 in blocking buffer, followed by a HRP-Avidin (Zymed, CA) in TBST containing 10% skim milk. The HRP signal was developed with Western Lighting™ and Western Lighting Plus Chemiluminescence Reagent (Perkin Elmer, MA) and the intensity of the bands were visualized by LAS image 4000 (Fujifilm, Japan). Quantitative assessments of the relative intensity of the blots were performed with NIH ImageJ.

Results

Preparation of EC-Fc protein

EC-Fc fusion protein was designed as EC-1 peptide fused to the amino terminus of IgG Fc domain (Fig. 1A). EC-Fc protein secreted from recombinant CHO cells were immunoprecipitated with protein A-agarose. The bound proteins were analysed by Western blotting with anti-human IgG to detect the Fc domain. As shown in Figure 1B, EC-Fc was observed as a monomer at approximately 30 kDa under reducing condition, whereas dimer at approximately 60 kDa was observed together with the tetramer, hexamer and higher order of oligomeric forms under non-reducing condition in either Coomassie Brilliant Blue (CBB) staining or Western blotting. The Fc domain without EC moiety prepared as a control was also observed as monomer at approximately 30 kDa under reducing condition, whereas only dimer formed as a result of the S-S-bond in the hinge region was observed at approximately 60 kDa under non-reducing condition. No further oligomeric forms were observed for Fc. These results suggested that the hinge region in the Fc domain should be effective to prepare dimeric form of Fc and EC-Fc proteins through disulfide bonds. The oligomeric forms observed as tetramer, hexamer and higher order can be because of the intermolecular disulfide bonds between cysteine residues in each EC-1 peptide. It is worthwhile noticing that no trimers were observed probably because extra-disulfide linkages were formed only between the EC-1 moieties of each EC-Fc proteins. The reduced protein in the CBB staining and Western blotting indicated an increment in the theoretical size of the artificial ligands, Fc and EC-Fc, which could be attributed to the N-linked glycosylation of the Fc portion of the human IgG. In this context, the oligomers should have two EC-1 moieties as correctly cyclized peptide through disulfide bonds in a molecule (Fig. 1C). The majority of EC-Fc was considered divalent form of EC-1 peptide even if the oligomeric forms such as hexamer and higher oligomer were formed because high oligomerization should precipitate EC-Fc and prevent it from working as ligand of ErbB2. For the susceptibility to the reducing conditions, EC-Fc was treated with DTT at various concentrations ranging from 0.5 to 5 mM at 4°C and 25°C (Fig. 1D). As the result, no order of disulfide bonds appeared to be present in the sensitivity to the reduction reagent in oligomeric forms because the reduction did not stop at a dimer even in low concentration of DTT. The specific binding affinity of EC-Fc to sErbB2 was evaluated by competition EIA (Fig. 1E). Scatchard plot revealed a high affinity binding site with a Kd of 26 nM, whereas a low affinity site was estimated to be 360 μM.

Internalization of ErbB2 was induced by EC-Fc in SK-BR-3 cells

Because the specific binding of EC-Fc to ErbB2 was confirmed, we then checked uptake of ErbB2 upon incubation with EC-Fc. For this assay, surface biotinylated cells were prepared and used. After incubation with EC-Fc, the biotin-labelled molecules retained on the cell surface were stripped off by the reducing reagent, whereas the molecules internalized were kept labelled with biotin so that they should be immunoprecipitated for the further analysis. The anti-ErbB2 antibody sc-08, which is known to induce internalization of ErbB2 in either SK-OV-3 cells or SK-BR-3 cells [13, 34], was used as a positive control. When evaluated on SK-BR-3 cells, EC-Fc was found to induce the internalization of ErbB2 (Fig. 2A). This internalization was estimated approximately 50% of that induced by anti-ErbB2 antibody sc-08. Internalized ErbB2 was observed when SK-OV-3 cells were treated with EC-Fc (Fig. 2B). In SK-OV-3 cells, the internalized ErbB2 induced by EC-Fc was almost equivalent with that induced by antibody sc-08. EC-Fc at 1 μM showed internalization of ErbB2 equivalent to that induced by anti-ErbB2 antibody sc-08 at 6.67 nM. This internalization was dependent on the doses of EC-Fc in a similar manner of monovalent EC-1 peptide fused to eGFP (EC-eGFP) [24]. When the biotinylated cells were treated with 5 μM EC-Fc, the internalized fraction of ErbB2 was increased up to three folds compared to that of the untreated cells at 37°C (Fig. 2C). We previously described that the internalization of ErbB2 was only observed in SK-OV-3 cells, when SK-BR-3 cells and SK-OV-3 cells were treated with EC-eGFP [24]. Taking the internalization demonstrated previously into consideration, this level of internalization was conceivable in SK-OV-3 cells, so that 5 μM EC-Fc should correspond to 10 μM EC-eGFP. The dimeric form of EC-Fc induced ErbB2 internalization whereas with EC-eGFP treatment ErbB2 was retained on the surface of the SK-BR-3 cells without internalization.

Internalization of ErbB2 was enhanced by multivalent form of EC-Fc in SK-BR-3 cells

The multivalent form of EC-1 peptide was prepared exploiting the affinity of ZZ-BNC for IgG Fc region (Fig. 3A). When ZZ-BNC was mixed with EC-Fc, the ligand EC-1 was multivalently displayed on the surface of ZZ-BNC (EC-Fc/BNC). On the other hand, ZZ-BNC displaying null ligand was just prepared by mixing Fc protein with ZZ- BNC (Fc/BNC). First of all, binding capacity and binding efficiency of the ZZ-BNC with ligand was optimized and characterized. To optimize the ratio of Fc fusion molecule to BNC, FITC-labelled

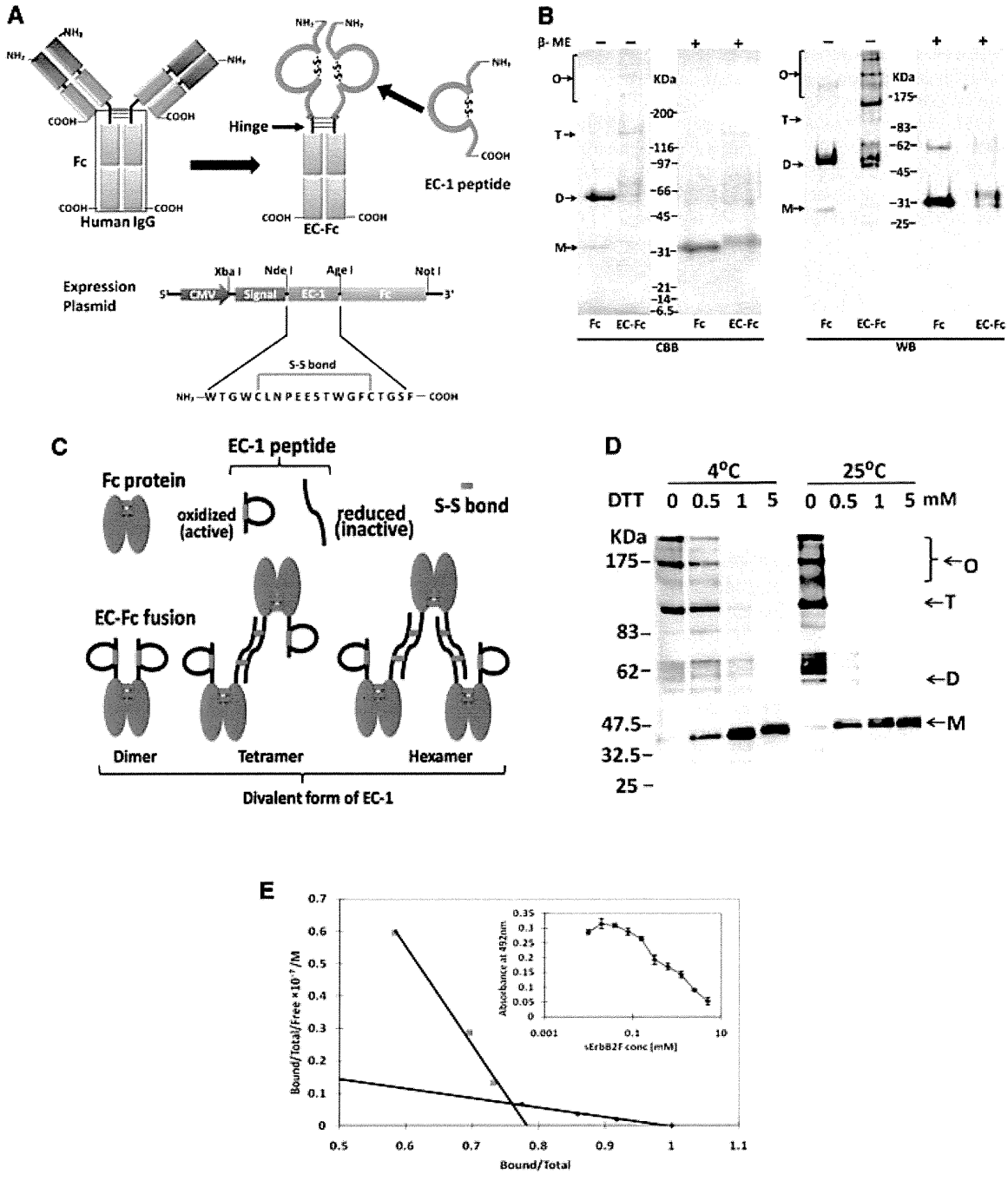

Fig. 1 Construction and preparation of EC-Fc. (**A**) Schematic diagrams of EC-Fc. EC-1 peptide was fused to the human IgG Fc domain containing hinge region, so that the fusion protein EC-Fc should form dimer. The secretional expression of EC-Fc was designed with the signal peptide derived from human RNase I under the control of CMV promoter. The unique restriction enzyme sites Xba I, Nde I, Age I and Not I were used to construct the expression plasmid. (**B**) EC-Fc (theoretical MW = 30.0 kDa) or IgG Fc (theoretical MW = 27.6 kDa) was produced, purified with protein A-column and subjected to SDS-PAGE and Western blotting. Anti-human IgG Fc antibody recognized the purified EC-Fc without significant degradation. β-ME: betamercaptoethanol; CBB: Coomassie Brilliant Blue staining; WB: Western blotting. (**C**) Reduction of EC-Fc oligomeric form with DTT treatment. WB: Western blotting; M: monomer; D: dimer; T: tetramer; O: oligomer (**B**, **C**). Molecular weight markers range from 6.5 to 200 kDa (**B**, **C**). (**D**) Schematic representation of the probable dimer, tetramer and hexamer formation of EC-Fc and dimer formation of Fc through disulphide linkages. (**E**) Evaluation of the affinity of EC-Fc for ErbB2 by competitive EIA. Kd values between EC-Fc and sErbB2F were estimated from the Scatchard plots.

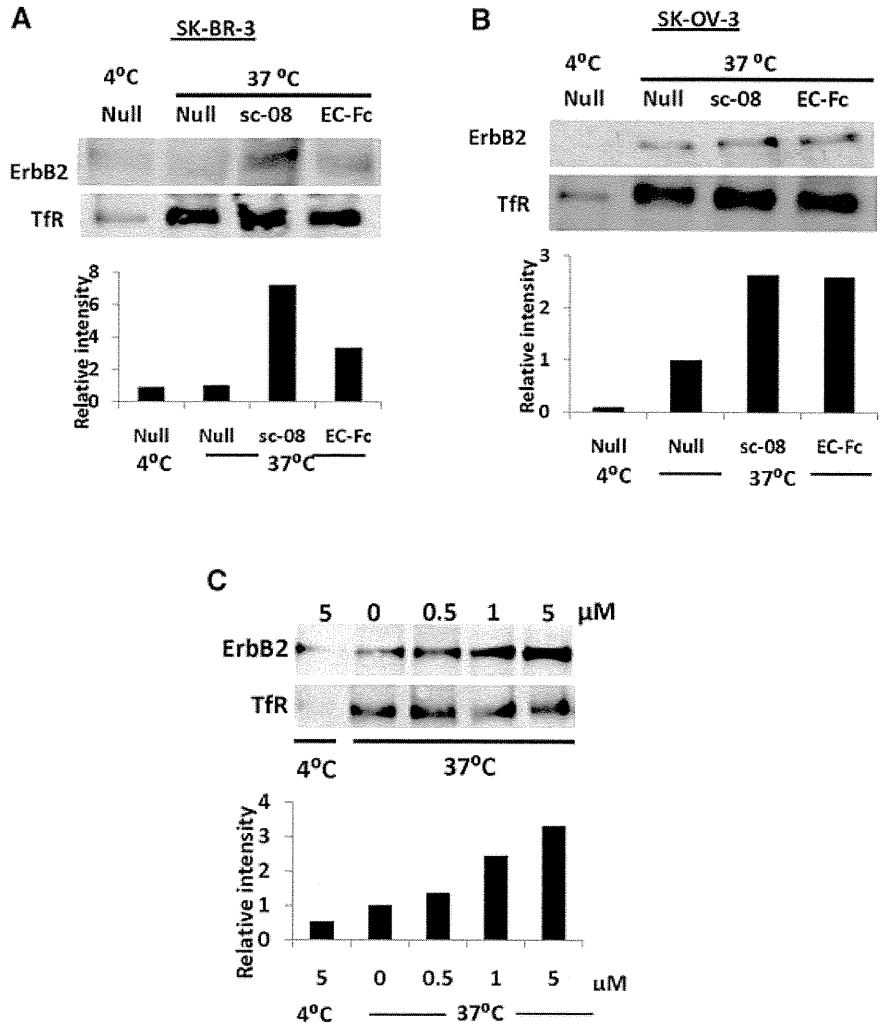

Fig. 2 Uptake of ErbB2 in SK-BR-3 and SK-OV-3 cells. The surface of SK-BR-3 cells (**A**) and SK-OV-3 cells (**B**, **C**) were labelled with biotin and were stimulated with EC-Fc. After treatment with trypsin internalized ErbB2 was immunoprecipitated with Avidin agarose and detected with HRP-labelled Avidin. (**A**, **B**) Cells were incubated at 4°C and 37°C without stimulation (Null), stimulated with antibody sc-08 for 1 hr and incubated with anti-mouse IgG for another 1 hr at 37°C (sc-08) and stimulated with EC-Fc 2 hrs at 37°C (EC-Fc). (**C**) SK-OV-3 cells were treated with various concentrations of the EC-Fc starting from 0 to 5 μM at 37°C and incubated at 4°C without stimulation for 2 hrs. Transferrin receptor (TfR) was monitored simultaneously as the control for the internalization experiments. This data set represents the representative of two independent experiments. The intensity of ErbB2 was densitometrically analysed by ImageJ and plotted into each graph to evaluate internalization. The density from the cells left untreated at 37°C was normalized as 1 in each graph.

ZZ-BNC was mixed with Fc protein at variable molar ratios of 1:10, 1:20, 1:40, 1:60, 1:80 and 1:100, respectively, and the residual fluorescent intensity in the supernatant was measured. As shown in Figure 3B, the soluble Fc/BNC was reduced to 30% at a molar ratio of ZZ-BNC to Fc protein at 1:100 when judged from the fluorescence in the supernatant. Similarly, when human IgG was used, the soluble IgG/BNC was found reduced to 10% at a molar ratio of ZZ-BNC to IgG protein at 1:100. The amount of Fc protein bound to ZZ-BNC in the supernatant was further estimated from intensity of the band detected by Western blotting (Fig. 3C). As the result, the amount of Fc protein bound to ZZ-BNC was determined maximum when the molar ratio of ZZ-BNC to Fc protein was at 1:20. Thus, EC-Fc/ZZ-BNC was prepared by mixing ZZ-BNC and EC-Fc at the molar ratio of 1:20 for further experiments.

ErbB2 internalization mediated by EC-Fc/BNC was evaluated by the cellular uptake of EC-Fc/BNC (Fig. 3D–F). The SK-BR-3 cells were incubated with either EC-Fc/BNC or Fc/BNC for 5 hrs at 37°C or 4°C (Fig. 3D). As a result, EC-Fc/BNC showed significant cellular uptake at 37°C in SK-BR-3 cells. The EC-Fc/BNC cellular uptake into SK-BR-3 cells was found not only dose dependent in the range from 1 to 10 nM (Fig. 3E) and time course dependent up to 8 hrs at 2 nM (Fig. 3F). These results suggest that multivalent EC-1 peptide displayed on BNC might make its internalization into the cells efficient. The time course changes in the internalization of BNC in SK-BR-3 cells were evaluated by incubating cells with EC-Fc/BNC for various time periods under a confocal microscope (Fig. 3G). To demonstrate that observed localization or internalization of the receptor is not an artefact of fixation and cell permeabilization, we assessed the internalization of the EC-Fc/BNC with live cell imaging (Fig. S1). The colocalization of EC-Fc/BNC was confirmed by merging the location of BNC and EC-Fc, whereas Fc/BNC did not show any internalization. The internalization of ErbB2 induced by EC-Fc/BNC was further confirmed under confocal microscope (Fig. 3H). SK-BR-3 cells were incubated with RITC-labelled BNC displaying EC-Fc at 2 nM for 4 hrs. Then the cells were further probed for the ErbB2 by anti-ErbB2 monoclonal antibody sc-08 followed by Alexa 488–labelled secondary antibody. The internalized ErbB2 was observed to be colocalized

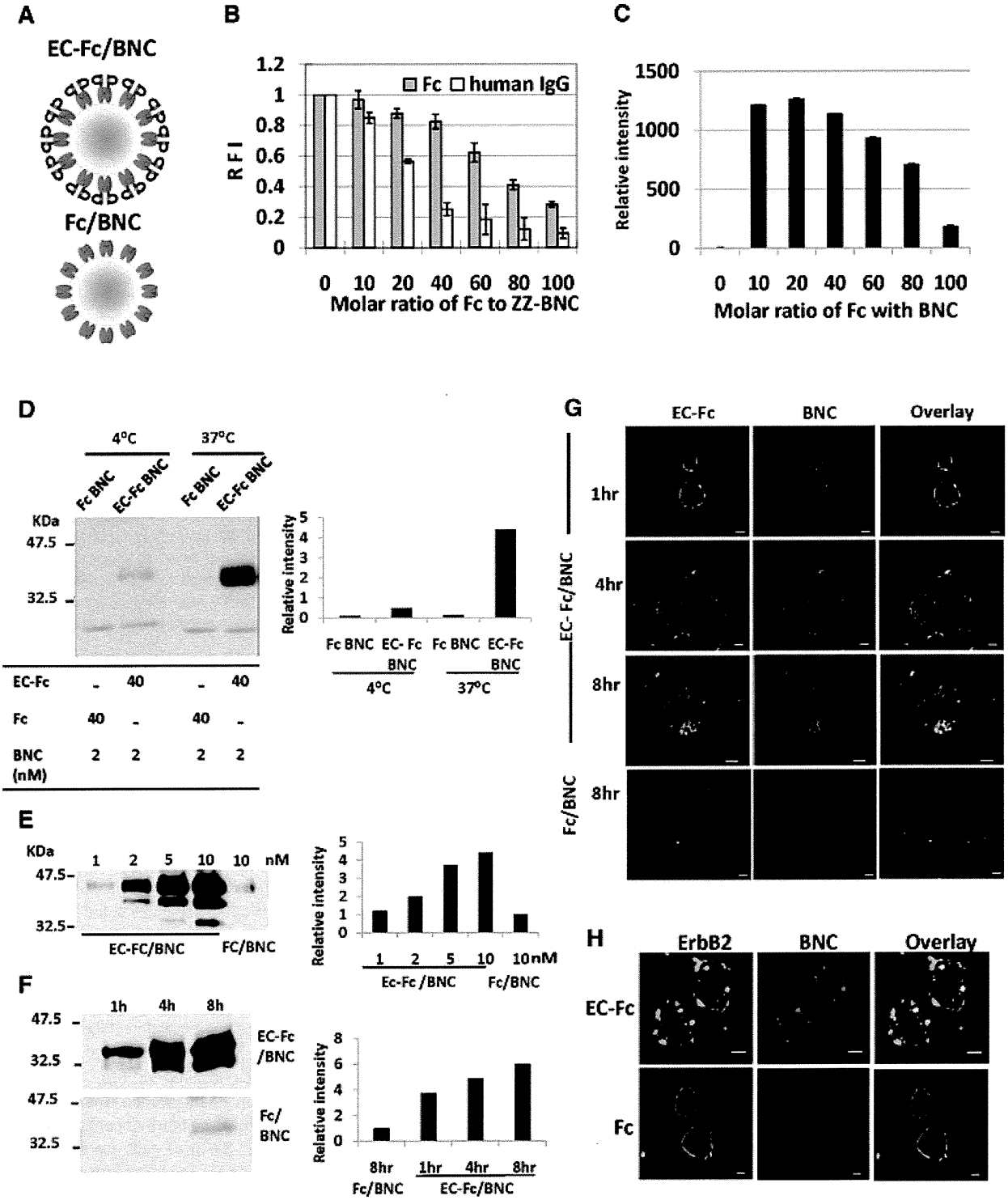

Fig. 3 Characterization of BNC displaying EC-Fc. (**A**) Schematic representation of the multivalent display of EC-Fc on ZZ-BNC (EC-Fc/BNC) and Fc on ZZ-BNC (Fc/BNC). (**B**) The solubility of BNC-displaying Fc/BNC and IgG/BNC was evaluated with FITC-labelled BNC. Residual fluorescence in supernatant was measured in varying molecular ratio of Fc or human IgG to ZZ-BNC. The intensity from the FITC-labelled ZZ-BNC without Fc was calculated as 1 in each graph. (**C**) Western blot analysis of Fc in the supernatant obtained in (**B**). Fc/BNC in the supernatant was immunoprecipitated with anti-HBsAg antibody conjugated to micro beads and was subjected to Western blotting. The Fc on the blot was detected with anti-human IgG. The bands were densitometrically analysed with ImageJ and relative intensity of each lane was plotted. (**D**–**F**) Assessment of internalization of EC-Fc/BNC in SK-BR-3 cells through Western blot. (**D**) EC-Fc/BNC (40 nM/2 nM) or Fc/BNC (40 nM/2 nM) was incubated with SK-BR-3 cells for 5 hrs at 4°C and 37°C. (**E**) SK-BR-3 cells were treated with various concentration of EC-Fc/BNC from 1 to 10 nM. Fc/BNC in 10 nM was taken as control. (**F**) SK-BR-3 cells were treated with 2 nM EC-Fc/BNC at various time periods. Simultaneously 2 nM Fc/BNC was taken as control. (**D**–**E**) After the incubation the cells were trypsinised and lysed followed by immunoprecipitation with anti-HBsAg antibody conjugated to micro beads. The precipitates were immunoblotted and were detected with anti–pre-S1 antibody. The bands of BNC were densitometrically analysed by ImageJ and plotted into each graph to evaluate amount endocytosed. (**G**, **H**) Confocal microscopic observation of SK-BR-3 cells treated with EC-Fc/BNC or Fc/BNC. Cells were incubated for various time periods (**G**) and for 4 hrs (**H**). The RITC-labelled ZZ-BNC was used and the cells were fixed and permeabilized. EC-Fc or Fc were detected with anti-human IgG labelled with FITC (**G**) and ErbB2 was detected with sc-08 antibody followed by rabbit anti-mouse IgG Alexa 488 (**H**). Bars, 10 μm.

together with BNC in SK-BR-3 whereas the Fc/BNC did not show any detectable internalization of ErbB2 as well as for BNC. As the result, the internalization of ErbB2 is concluded to be dependent on the uptake of BNC displaying EC-1 peptide multivalently. Internalization of EC-Fc/BNC was found to be dependent on both time course and ErbB2 in SK-BR-3 cells. Simultaneously, the internalization of ErbB2 was confirmed to be induced when EC-Fc/BNC was added. This observation implies that the cellular uptake of EC-Fc/BNC should be associated with the receptor-mediated endocytosis.

Comparative study of the effect by EC-Fc and EC-Fc/BNC

The specific binding of EC-1 ligand to cells overexpressing ErbB2 was assessed by immunostaining (Fig. 4A). Three cell lines MCF-7, SK-BR-3 and SK-OV-3 cells were selected and the binding of EC-Fc protein and EC-Fc/BNC was evaluated. The expression level ErbB2 was approximately 10^4 sites/cell in MCF-7 [30], 10^6 sites/cell in SK-BR-3 and SK-OV-3, respectively [31, 32]. The cells were incubated with EC-Fc or Fc or EC-Fc/BNC or Fc/BNC for 1 hr at 37°C followed by staining with anti-human IgG Fc-labelled with FITC. The fluorescence was observed only at the linage of SK-BR-3 and SK-OV-3 cells but not with MCF-7 whereas Fc and Fc/BNC did not show any positive staining in all cell lines. No detectable fluorescence at the confocal microscopy to MCF-7 attributes to the low ErbB2 expression in the cells. The surface binding of the EC-Fc/BNC as well as EC-Fc was then qualitatively analysed by flow cytometry. As shown in Figure 4A in SK-BR-3 and SK-OV-3 cells, EC-Fc (green line) as well as Ec-Fc/BNC (blue line) exhibited to bind to cell surface specifically. The binding efficiency of EC-Fc was found to be better than EC-Fc/BNC for SK-BR-3 cells. As the results, the specific binding of EC-Fc and EC-Fc/BNC to ErbB2 and overexpressing cells was successfully demonstrated.

ErbB2 internalization depending on the doses of EC-Fc and EC-Fc/BNC was assessed in the range of 20–200 nM in SK-BR-3 cells (Fig. 4B). ErbB2 internalization was observed with both EC-Fc and EC-Fc/BNC. When the intensity of the band analysed densitometrically showed the internalization of ErbB2 was more efficient by the stimulation for 2 hrs up to 100 nM of the ligand multivalently displayed on BNC than by EC-Fc ligand alone (Fig. 4C).

EC-Fc/BNC internalized through GEEC pathway in SK-BR-3 cells

Cells adopt divergent pathways for the endocytosis of the cargos and receptors. The key pathways were categorized into clathrin-dependent and clathrin-independent mechanisms [33]. The clathrin-independent pathway is further classified into caveolar and GPI-anchored early endocytic compartments (GEEC) pathways [33, 34]. ErbB2 is thought to be internalizing in SK-OV-3 through clathrin-mediated internalization [24]. In this study we found that the mechanism of internalization of ErbB2 present in SK-OV-3 cells is deficient in SK-BR-3 cells. We tried to identify the difference between the two cell lines using DNA microarray (Fig. S2). As a result the expression of claudin 16, caveolin-1 and caveolin-2 were found to be extensively down-regulated in SK-BR-3 cells when compared to SK-OV-3 cells. This absence of caveolin-1 in SK-BR-3 cells was further confirmed by immunostaining using anti-Cav1 antibody (Fig. 5A). SK-BR-3 did not show the presence of caveolin-1 suggesting that the impaired caveolar mechanism prevailing in the cell, which was consistent with the finding by the previous reports [13, 35]. Because caveolin-1 was detected in SK-OV-3 cells the internalization pathway deficient in SK-BR-3 cells might be attributed to caveolae.

The mechanistic approach for the uptake of the EC-Fc/BNC was assessed in SK-BR-3 cells using inhibitors for other pathways. SK-BR-3 cells were treated with EC-Fc/BNC in the presence or absence of inhibitors for clathrin, and GEEC pathway and the internalization was assessed. When the cells were treated with 100 nM CPZ, an amphiphilic drug, which inhibits the clathrin-mediated pathway, the internalization of the EC-Fc/BNC was unaffected (Fig. 5B).

Most of the cargos irrespective of their route merges with Rab5 and early endosome antigen-1 (EEA-1) enriched in early endosomes, which is further sorted into various intracellular destinations [36, 37]. The colocalization of EC-Fc/BNC with EEA-1 was assessed with anti–EEA-1 antibody under confocal microscope at various time periods starting from 5, 30 and 90 min and the colocalization was found to be maximum at 30 min (Fig. S3).

When the cells were treated with 5 mM mβCD, which dislodges the cholesterol from the surface and inhibit the cdc42 activity, for 30 min the internalization was blocked and the cells untreated showed considerable uptake of EC-Fc/BNC. The bound fractions of EC-Fc/BNC were treated with and without acid stripping to ensure the colocalized fraction inside the cells (Fig. 5C). The colocalization was calculated to more than 60%, which was reduced in the internalization of EC-Fc/BNC with the mβCD treatment. To assess the surface binding of the EC-Fc/BNC after the inhibitor treatment the cells were stained for the ErbB2 and EC-Fc/BNC at various concentration of the mβCD (Fig. S4). The inhibitor treatment did not deteriorate the binding affinity of the EC-Fc/BNC to ErbB2. These results were further confirmed with flow cytometric studies (Fig. S5).

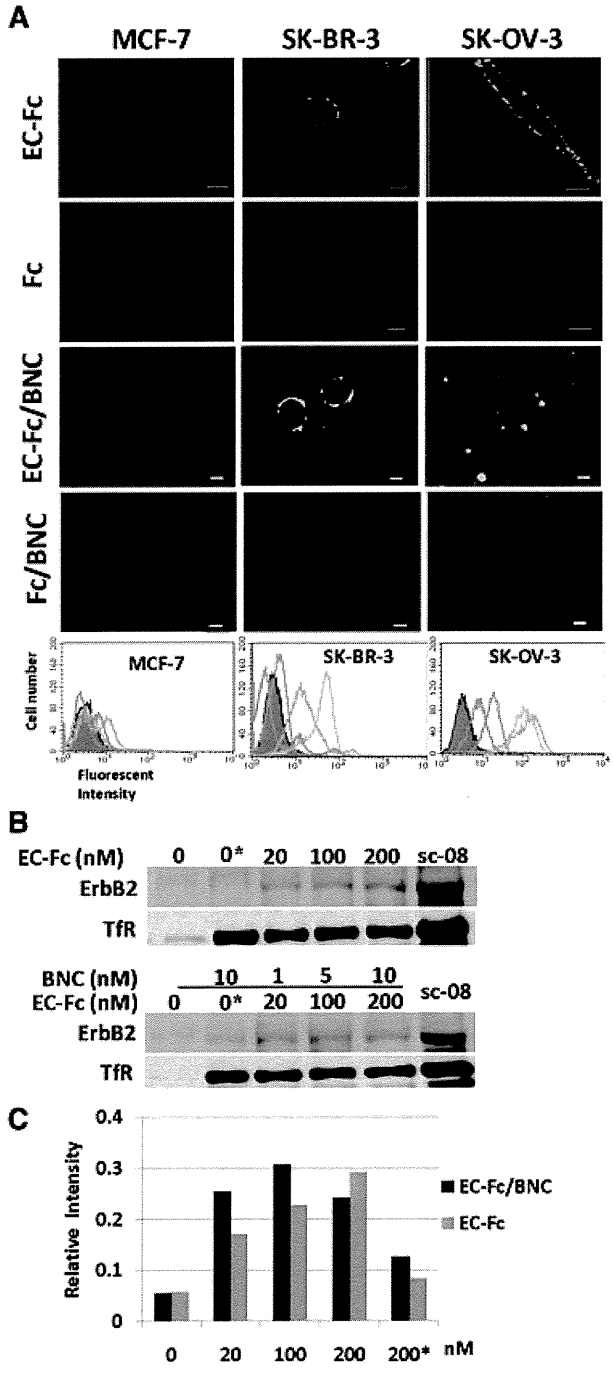

Fig. 4 Evaluation of ErbB2 internalization in SK-BR-3 cells treated with EC-Fc/BNC. (**A**) Comparison of EC-Fc/BNC bound to the surface of the cells over expressing ErbB2. Cells were incubated with EC-Fc (1 μM), Fc (1 μM), EC-Fc/BNC (40 nM/2 nM), and Fc/BNC (40 nM/2 nM) for 1 hr at 37°C in MCF-7 cells, SK-BR-3 cells, and SK-OV-3 cells. MCF-7 cells were used as the control for low ErbB2 expression. The cells were stained with anti-human IgG labelled with FITC. Bars depict 10 μm. The treated cells were also subjected to flow cytometoric analysis for the surface bound fraction of EC-Fc and Fc ligand with and without BNC in MCF-7, SK-BR-3 and SK-OV-3, respectively. Untreated cells were shown in shadow (grey). Treatment with EC-Fc ligand Fc ligand, EC-Fc/BNC and Fc/BNC was marked as green, magenta, blue and orange, respectively. (**B**) SK-BR-3 cells were treated with different concentration of EC-Fc or Ec-Fc/BNC. The cell surface receptors were reversibly biotinylated with NHS-SS-Biotin and were incubated with EC-Fc, Fc, EC-Fc/BNC or Fc/BNC for 2 hrs at 37°C. SK-BR-3 cells left untreated at 4°C for 2 hrs were shown as lane '0'. '0*' corresponds to the cells treated with Fc ligand (top) and Fc/BNC (lower) at a concentration of 200 nM, respectively. After the treatments, cells were lysed, immunoprecipitated with avidin agarose and were subjected to Western blot to detect ErbB2 with anti-ErbB2 antibody. sc-08 antibody treatment was taken as positive control for endocytosis of ErbB2. Transferrin receptor (TfR) was monitored as an internal control for the experiments. (**C**) The bands from the Western blots were densitometrically analysed with ImageJ and the intensity each band was normalized by the intensity when treated with antibody sc-08.

Discussion

The EC-Fc was designed as dimer due to the hinge region in IgG Fc domain (Fig. 1A). However, we found higher oligomeric forms such as tetramer and hexamer. These higher order forms were supposed to be divalent as described in 'Results' and Figure 1C. Further multivalent form of EC-1 peptide was prepared by displaying EC-Fc on BNC which was optimized to a ratio of EC-Fc to BNC = 1:20. These divalent and multivalent forms of EC-Fc induced internalization of ErbB2 into SK-BR-3 cells whereas

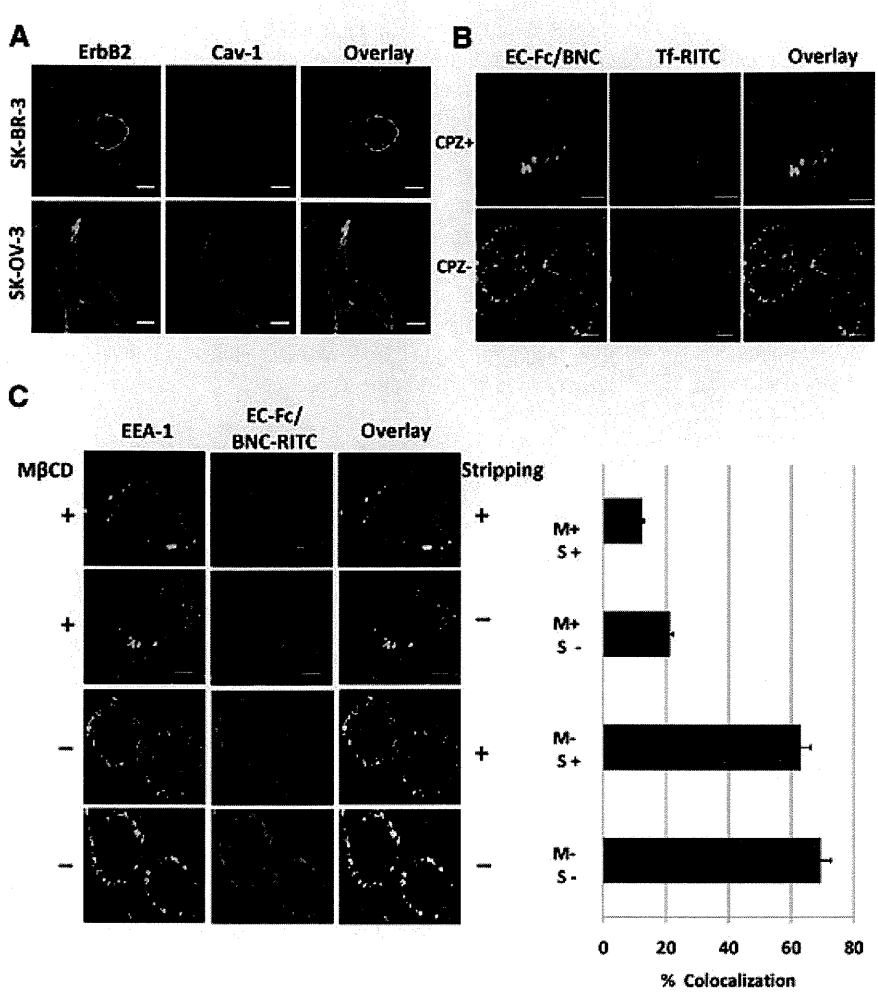

Fig. 5 Assessment of the mechanism of internalization of EC-Fc/BNC in SK-BR-3 cells. (**A**) SK-BR-3 cells and SK-OV-3 cells were stained with antibodies against ErbB2 (green) and Cav-1 (red). (**B**) SK-BR-3 cells were treated with EC-Fc/BNC in the presence or absence of 100 nM of CPZ and stained with anti-human IgG antibody labelled with FITC. Transferrin-RITC was used as a control for the internalization. (**C**) SK-BR-3 cells were treated with EC-Fc/BNC labelled with RITC in the presence or absence of mβCD. The cells were stained with anti–EEA-1 antibody followed by secondary antibody against mouse IgG labelled with AlexaFlour-488. The cells were then stripped with and without acid treatment to remove the surface bound fraction and to visualize the internalized fraction. Bars, 10 μm.

monovalent form of EC-1 peptide did not induce internalization [24]. The internalization of ErbB2 was found dependent on the concentration in the range of 20–200 nM for EC-Fc and appeared to be enhanced when 20–100 nM EC-Fc was displayed on BNC (Fig. 4B). EC-Fc/BNC appeared more efficient in inducing the internalization of ErbB2 when compared to EC-Fc ligand alone. The time course dependence of the BNC internalization was found to be also in the same range of EC-Fc/BNC concentration. The binding affinity of the EC-Fc was estimated to be about 26 nM whereas monovalent EC-1 peptide as EC-eGFP fusion showed 1 μM (Table 1). The affinity of the multivalent display for ErbB2 was 33 nM, which did not ameliorate the affinity of EC-Fc for the ErbB2. Therefore, the affinity should elucidate the enhanced internalization of ErbB2 induced by EC-Fc/BNC in SK-BR-3 cells. It is believed that the heterodimerization between ErbB2 and ErbB3 is one of the reasons for retention of ErbB2 on the cell surface, so that monovalent form of the EC-1 peptide could not induce internalization of ErbB2 in SK-BR-3 cells. Shuttling between homodimers and heterodimers should increase depending on the distance of the dimers. EC-Fc supposedly keeps the receptors close enough to facilitate homodimer formation, which will allow the internalization of ErbB2. Therefore, the cells treated with EC-Fc/BNC showed considerable increment in the internalization of

Table 1 Affinity for ErbB2 of EC-1 peptide in various forms and internalization of ErbB2 in SK-OV-3 and SK-BR-3 cells

Forms of EC-1 peptide	EC-eGFP	EC-Fc	EC-Fc/BNC
Kd (nM)	1.0×10^{3}*	2.6×10	3.3×10
Internalization of ErbB2 observed in			
SK-OV-3 cells	+†	++‡	++
SK-BR-3 cells	–§	+	++

*[24].
†Internalization was observed in the range of μM orders of ligands.
‡Internalization was observed in the range of nM orders of ligands.
§Internalization was not observed.

the BNC, although the effect of EC-Fc moiety appeared conceivable because Fc/BNC did not show significant internalization of ErbB2 as the background (Fig. 3D–F).

It is thought that the processing and degradation of the ErbB2 is different in various cell lines [24, 34, 35]. The CPZ at 100 nM, which inhibits the formation of clathrin-coated pits, inhibited the internalization of ErbB2 by EC-1 peptide fused to eGFP in SK-OV-3 [24]. On the contrary, the same concentration of CPZ did not block the internalization of ErbB2 in SK-BR-3 cells. In this study, we confirmed the absence of caveolin-1 in SK-BR-3 cells using microarray and immunostaining where it showed around 300-fold increment in the expression of Cav-1 in SK-OV-3 cells (Fig. S1). Recent studies support our observation that the SK-BR-3 cells lack caveolae [13, 35]. ErbB2 internalization after geldanamycin treatment showed GEEC or clathrin-independent compartments (CLIC) pathway, which ultimately fuses with the classical pathway for the degradation in lysosomes, is independent of caveolar and clathrin pathway [35].

In this study we employed mβCD, a cholesterol dislodging oligosaccharide, for deciphering the mechanism behind the internalization of the EC-Fc/BNC in SK-BR-3 cells, as an inhibitor for the blockade of GEEC pathway. Cholesterol depletion with mβCD inhibits both caveolar [38] and GEEC pathway [39, 40]. Earlier it was shown that cholesterol level determines the internalization of GPI-anchored proteins and with clostridium difficile toxin B [34, 39]. Because SK-BR-3 cells lack caveolar machinery, the blockade with mβCD will only correspond its effect in blocking the internalization of GEEC-mediated mechanism. The internalization of ErbB2 is sensitive to the depletion of cholesterol, which is essential for most of the clathrin-independent pathways. GEECs are formed as compartments free of clathrin, caveolin and dynamin, which are short lived (2–5 min) and ultimately fuses with EEA-1 enriched early endosome [33, 38]. It was shown that cdc42 is responsible for the dynamin-dependent and clathrin-independent internalization of GPI-anchored proteins. It was also reported earlier that cdc42 activation recruits actin polymerization machinery rendering this pathway sensitive to inhibitors of cholesterol depletion and actin polymerization [39]. This pathway specifies the visible difference in the uptake of the EC-Fc/BNC between SK-OV-3 and SK-BR-3 cells.

Another important molecule, which plays a key role in the GEEC pathway, is EEA-1 that contains an FYVE finger, which interacts with PI3K [41, 42]. PI3K phosphorylates Rab 5 that helps the EEA-1 to localize to early endocytic compartments [36]. The colocalization of EC-Fc/BNC with EEA-1, which corresponds the preliminary step in the endosomal pathways before transferring it to the sorting endosomes, was observed (Fig. S2). Because both caveolar and clathrin pathways are impaired in SK-BR-3 cells as described earlier, the colocalization should correspond to GEEC pathway.

In this study, we revealed the presence of GEEC pathway as ErbB2 internalization, which critically differs between SK-BR-3 cells and SK-OV-3 cells using EC-1 peptide in various forms. As for the nanoparticle internalization, the pathways of clathrin and caveolar- independent endocytosis have not been described until now [43]. The internalization of the carrier particle was described repeatedly on folate receptor (FR) tagged nanoparticles [44]. In these reports, mechanism of the carrier internalization emphasizes the FR internalization through GEEC pathway. Similarly, EC-Fc should utilize the mechanism of internalization of ErbB2 in this study even when they are displayed on BNC (Fig. 4B).

It is considered that ZZ-BNC is an efficient nano-machine for molecular targeting in drug delivery system displaying antibodies on the surface [25, 29, 45]. Multivalency of EC-Fc was successfully demonstrated to target ErbB2 enhancing the internalization of ErbB2, in this report. In this context, delivery of therapeutic substances into specific cells of various diseases including cancer can be feasible if EC-Fc/BNC is used as a drug delivery system. Multivalent display strategy proposed here should be useful for molecular targeting to introduce therapeutic drug into the cells followed by the internalization of receptors.

Acknowledgements

The authors thank Prof. N. Kanayama for his valuable help and suggestions in flow cytometric analysis. The authors also thank Prof. H. Matsui for helpful discussion throughout the work. This work was partly supported by Grant-in-Aid for Scientific Research (B) from the Ministry of Education, Culture, Sports, Science and Technology (No. 21300179) in Japan, Health and Labor Sciences Research Grants, Research on Nanotechnical Medical, H21-nano-general-004 and National Natural Science Foundation of China (Key Program, Grant No. 30930038).

Conflict of interest

The authors report no conflicts of interest. The authors alone are responsible for the content and writing of the paper.

Supporting information

Additional Supporting Information may be found in the online version of this article:

Fig. S1 Live cell imaging. For live cell imaging, the SK-BR-3 cells were cultured in 18 mm coverslips and washed twice with phenol red free RPMI (Sigma) containing 1 % glucose, 25 mM HEPES and 1 % BSA supplemented with 100 U/ml pencillin and 100 μg/ml streptomycin. The EC-Fc BNC tagged with RITC was incubated on ice for 30 min prior to the visualization in order to enable the binding of the multivalent forms of BNC to the cell surface. The cells were then washed thrice with warm media and were visualized in 100X 1.3 N.A. oil immersion objectiveunder Olympus IX81 inverted microscope (Olympus) with temperature control followed by data acquisition with Metamorph software (Molecular Devices). The imaging was carried out with DP71 cooled CCD camera attached to the microscope and the fluorescence of RITC was acquired along with the DIC field image. The time-lapse imaging

was carried out for one hour with time intervals of 5 minutes each. In Metamorph software, each channel was split and overlayed separately. The acquired stacks were analyzed with MBF Image J.

Fig. S2 Microarray analysis. Expression of genes in SK-BR-3 cells was analyzed by microarray procedure. Total RNA preparation and analysis was performed as described previously [46, 47]. DNA microarray was carrying 1,795-oligonucleotide probes for human cell surface proteins. cDNAs were synthesized with Superescript II reverse transcriptase (Invitrogen) with oligo dT primers. Amino-allyl-dUTP was incorporated into cDNAs followed by coupling with Cy-3 dye (Ambion, TX, USA) and were processed for hybridization at 55°C for 15 hours. The fluorescent images for the hybridization were captured using FLA8000 scanner (Fuji Film, Japan) and analyzed with GenePix Pro5.1 software (Axon Instruments, CA). We found caveolins, Cav-1 and 2, and claudin 16 (CLDN-16) were downregulated in SK-BR-3 cells when compared to SK-OV-3 cells while ErbB2 and GAPDH expression were equally expressed in both the cell lines. RT-PCR (Fig. S1A) and qRT-PCR (Fig. S1B) further confirmed these results. The conditions for the RT-PCR are as follows: 94°C for 5min; followed by 30 cycles of 94°C for 30 sec, 55°C for 30 sec, 72°C for 30 sec and 72°C for 7 minutes. Quantitative real time PCR was performed with SYBR Green Realtime Master Mix (Toyobo) in triplicates containing 5ng of cDNA along with 400 nM primers using LightCycler™ (Roche). The thermal cycling condition was as follows: 95°C for 1 min followed by 40 cycles of 95°C -10 sec, 55°C for 10 sec, 72°C for 25 sec and 60°C for 1 min. The following sets of the primers were used for the PCR reaction. Claudin-16, (Forward) 5′- GCTTGCCACAATGAGGGATCT-3′, (Reverse) 5′-TGACTTGGCCATGGAAACACC-3′; Cav-1 (Forward) 5′-GACTCG-GAGGGACATCTCTAC-3′, (Reverse) 5′-GTTGATGCGGACATTGCTGA-3′; Cav-2, (Forward) 5′-ACGTACAGCTCTTCATGGAC-3′ (Reverse) 5′-CAGTTGCAGGCTGACAGAAG-3′.

Fig. S3 Time dependent colocalization of EC-Fc BNC in early endosomes. Colocalization of EC-Fc/BNC-RITC with EEA-1 was found in the early endosomes. SK-BR-3 cells were treated with EC-Fc/BNC-RITC for 5, 30, 90 min, and the colocalization of the EC-Fc/BNC-RITC with the early endosomal marker, EEA-1 was assessed with anti EEA-1 antibody (BD Biosciences) and the secondary antibody labeled with AlexaFlour-488 (Molecular Probes). Error bars indicate standard error. JACoP plugin in Image J was employed for percentage colocalization assessment. Percentage colocalization was found to be maximum up to approximately 70% by 30 min. The data represented here is the representative of two independent experiments.

Fig. S4 Binding of EC-Fc BNC to the cell surface after treatment with varying concentration of mβCD. The binding of EC-Fc/BNC's to ErbB2, in the presence of 2 to 10 mM of cholesterol dislodging oligosaccharide-mβCD, was not affected. SK-BR-3 cells were treated with 5 and 10 mM of mβCD for 30 minutes followed by treatment with EC-Fc/BNC labeled with RITC are shown in Figure S2. The cells were stained with anti ErbB2 antibody (green) and red spots indicate EC-Fc/BNC labeled with RITC. Bars depict 10 μm.

Fig. S5 FACS analysis for the surface binding and internalization of EC-Fc BNC with inhibitor treatment. Surface binding and internalization of EC-Fc/BNC labeled with FITC in SK-BR-3 cells was quantified using FACS analysis. First, the binding of EC-Fc/BNC on SK-BR-3 cells was treated with or without 5 mM of mβCD on ice for 30 min. The cells were then fixed and analyzed with FACS to determine the surface bound fraction (Fig. S5A). The histograms showed overlapping of the peak tops indicating that the surface binding is majorly unaffected by the mβCD treatment. The peak (blue), which corresponds to approximately 20% of the total cell counts, orienting towards the untreated cells (grey peak) indicates the presence of a different population of cells that are incapable of binding to EC-Fc/BNC after mβCD treatment. Simultaneously, another set cells were treated with EC-Fc/BNC labeled with FITC in the presence or absence of 5 mM of mβCD at 37°C for 30 minutes. Cells were then trypsinized to remove the surface fraction, fixed and permeabilized, and the internalized fraction was analyzed adopting the same procedure with FACS (Fig. S5B, C). mβCD treated SK-BR-3 cells showed a peak point in the histogram which overlaid the peak area of untreated cells indicating the mβCD inhibits the internalization, while the cells without mβCD treatment drifted from the untreated cells towards the right. Total intensity of the internalized fraction was assessed from the FACS data were plotted on to a graph (Fig. S5). mβCD suppressed the internalization to approximately 50% when compared to the absence of mβCD treatment. M: mβCD; T: trypsin. Error bars indicate standard error.

Please note: Wiley-Blackwell is not responsible for the content or functionality of any supporting information supplied by the authors. Any queries (other than missing material) should be directed to the corresponding author for the article.

References

1. **Yarden Y, Sliwkowski MX.** Untangling the ErbB signaling network. *Nature Rev Mol Cell Biol.* 2001; 2: 127–37.
2. **Olayioye MA, Neve, RM, Lane HA, *et al.*** The ErbB signaling network: receptor heterodimerization in development and cancer. *EMBO J.* 2000; 9: 3159–67.
3. **Klapper LN, Waterman H, Sela M, *et al.*** Tumor-inhibitory antibodies to HER-2/ErbB-2 may act by recruiting c-Cbl and enhancing ubiquitination of HER-2. *Cancer Res.* 2000; 60: 3384–8.
4. **Slamon DJ, Clark GM, Wong SG, *et al.*** Human breast cancer: correlation of relapse and survival with amplification of the HER-2/neu oncogene. *Science.* 1987; 235: 177–82.
5. **Hynes, NE, Stern DF.** The biology of ErbB2/neu/HER-2 and its role in Cancer. *Biochem Biophys Acta.* 1994; 1198: 164–84.

6. **De Placido S, Carlamangno C, De Laurentiis M, *et al.*** C-erbB2 expression predicts tamoxifen efficacy in breast cancer patients. *Breast Cancer Res Treat.* 1998; 52: 55–64.
7. **Pinkas-Kramarski R, Soussan L, Waterman H, *et al.*** Diversification of Neu differentiation factor and epidermal growth factor signaling by combinatorial receptor interactions. *EMBO J.* 1996; 15: 2452–67.
8. **Baselga J, Swain SM.** Novel anticancer targets: revisiting ERBB2 and discovering ERBB3. *Nat Rev Cancer* 2009; 9: 463–75.
9. **Salomon DS, Brandt R, Ciardiello F, *et al.*** Epidermal growth factor-related peptide and their receptors in human malignancies. *Crit Rev Oncol Ematol.* 1995; 19: 183–232.
10. **Slamon DJ, Godolphin W, Jones LA, *et al.*** Studies of the HER-2/neu proto-oncogene in human breast and ovarian cancer. *Science.* 1989; 244: 707–12.
11. **Zhang X, Silva E, Gershenson D, *et al.*** Amplification and rearrangement of c-erb B proto-oncogenes in cancer of human female genital tract. *Oncogene* 1989; 4: 985–9.
12. **Austin CD, De Maziere AM, Pisacane PI, et al.** Endocytosis and sorting of ErbB2 and the site of action of cancer therapeutics trastuzumab and geldanamycin. *Mol Biol Cell.* 2004; 15: 5268–82.
13. **Hommelgaard AM, Lerdrup M, van Deurs B.** Association with membrane protrusions makes ErbB2 and internalization-resistant receptor. *Mol Biol Cell.* 2004; 15: 1557–67.
14. **Lerdrup M, Brunn S, Grandal MV, *et al.*** Endocytic downregulation of ErbB2 is stimulated by cleavage of its C-terminus. *Mol Biol Cell.* 2007; 18: 3656–66.
15. **Lerdrup M, Hommelgaard AM, Grandal MV, *et al.*** Geldanamycin stimulates internalization of ErbB2 in a proteosome-dependent pathway. *J Cell Sci.* 2006; 119: 85–95.
16. **Hudziak RM, Lewis GD, Winget M, *et al.*** P185HER2 monoclonal antibody has antiproliferative effects *in vitro* and sensitizes human breast tumor cells to tumor necrosis factor. *Mol. Cell. Biol.* 1989; 9: 1165–72.
17. **Lewis GD, Lofgren JA, McMurtey AE, *et al.*** Growth regulation of human breast and ovarian tumor cells by heregulin: evidence for the requirement of ErbB2 as a critical component in mediating heregulin responsiveness. *Cancer Res.* 1996; 56: 1457–65.
18. **Cuello M, Ettenberg SA, Clark AS, *et al.*** Downregulation of the erbB2 receptor by trastuzumab (herceptin) enhances tumor necrosis factor related apoptosis inducing ligand mediated apoptosis in breast and ovarian cancer cell lines that overexpress erbB2. *Cancer Res.* 2001; 61: 4892–900.
19. **Baselga J, Albanell J, Molina MA, *et al.*** Mechanism of action of trastuzumab and scientific update. *Semin Oncol.* 2001; 28: 4–11.
20. **Urbanelli L, Ronchini C, Fontana L, *et al.*** Targeted gene transduction of mammalian cells expressing the HER2/neu receptor by filamentous phage. *J Mol Biol.* 2001; 313: 965–76.
21. **Karasseva NG, Glinsky VV, Chen NX, *et al.*** Identification and characterization of peptides that bind human ErbB2 selected from a bacteriophage display library. *J Protein Chem.* 2002; 21: 287–96.
22. **Houimel M, Schneider P, Terskikh A, *et al.*** Selection of peptides and synthesis of pentameric peptabody molecules reacting specifically with ErbB-2 receptor. *Int J Cancer.* 2001; 92: 748–55.
23. **Pero SC, Shukla GS, Armstrong AL, *et al.*** Identification of a small peptide that inhibits the phosphorylation of ErbB2 and proliferation of ErbB2 overexpressing breast cancer cells. *Int J Cancer.* 2004; 111: 951–60.
24. **Hashizume T, Fukuda T, Nagaoka T, *et al.*** Cell type dependent endocytic internalization of ErbB2 with an artificial peptide ligand that binds to ErbB2. *Cell Biol Int.* 2008; 32: 814–26.
25. **Tsutsui Y, Tomizawa K, Nagita M, *et al.*** Development of bionanocapsules targeting brain tumors. *J Control Release* 2007; 122: 159–64.
26. **Tada H, Kurokawa T, Seita T, *et al.*** Expression and characterization of a chimeric bispecific antibody against fibrin and against urokinase-type plasminogen activator. *J Biotech.* 1994; 33: 157–74.
27. **Seno M, Futami J, Kosaka M, *et al.*** Nucleotide sequence encoding human pancreatic ribonuclease. *Biochim Biophys Acta.* 1994; 1218: 466–8.
28. **Nagaoka T, Fukuda T, Hashizume T, *et al.*** A betacellulin mutant promotes differentiation of pancreatic acinar AR42J cells into insulin-producing cells with low affinity of binding to ErbB1. *J Mol Biol.* 2008; 380: 83–94.
29. **Yamada T, Iwasaki Y, Tada H, *et al.*** Nanoparticles for the delivery of genes and drugs to human hepatocytes. *Nat Biotechnol.* 2003; 21: 885–90.
30. **Dini M, Jafari K, Faiferman I.** Cell-mediated cytotoxicity in pre invasive and invasive squamous cell carcinoma of the cervix. *Obstet Gynecol.* 1980; 55: 728–31.
31. **Hughes DPM, Thomas, DG, Giordano TJ, *et al.*** Cell surface expression of epidermal growth factor receptor and Her-2 with nuclear expression of Her-4 in primary osteosarcoma. *Cancer Res.* 2004; 64: 2047–53.
32. **Friedman LM, Rinon A, Schechter B, *et al.*** Synergistic down-regulation of receptor tyrosine kinases by combinations of mAbs: implications for cancer immunotherapy. *Proc Natl Acad Sci.* 2005; 102: 1915–20.
33. **Mayor S, Pagano RE.** Pathways of clathrin-independent endocytosis. *Nat. Rev. Mol. Cell. Biol.* 2007; 8: 603–12.
34. **Kirkham M, Parton RG.** Clathrin-independent endocytosis: new insights into caveolae and non-caveolar lipid raft carriers. *Biochim Biophys Acta.* 2005; 1745: 272–86.
35. **Barr DJ, Ostermeyer-Fay AG, Matundan RA, *et al.*** Clathrin-independent endocytosis of ErbB2 in geldanamycin-treated human breast cancer cells. *J Cell Sci.* 2008; 121: 3155–66.
36. **Sönnichsen B, De Renzis S, Neilsen E, *et al.*** Distinct membrane domains on endosomes in the recycling pathway visualized by multicolor imaging of Rab4, Rab5, and Rab 11. *J Cell Biol.* 2000; 149: 901–14.
37. **Falcone S, Cocucci E, Podini P, *et al.*** Macropinocytosis: regulated coordination of endocytic and exocytic membrane traffic events. *J Cell Sci.* 2006; 119: 4758–69.
38. **Sabharanjhak S, Sharma P, Parton RG, *et al.*** GPI-anchored proteins are delivered to recycling endosomems *via* a distinct cdc42-regulated, clathrin-independent pinocytic pathway. *Dev Cell.* 2002; 2: 411–23.
39. **Chadda R, Howes MT, Plowman SJ, *et al.*** Cholesterol-sensitive Cdc42 activation regulates actin polymerization for endocytosis *via* the GEEC pathway. *Traffic.* 2007; 8: 702–17.
40. **Brown FD, Rozelle AL, Yin HL, *et al.*** Phosphatidylinositol 4,5-bisphosphate and Arf6-regulated membrane traffic. *J Cell Biol.* 2001; 154: 1007–18.
41. **Mu F-T, Callaghan JM, Steele-Mortimer O, *et al.*** EEA1, an early endosome-associated protein. EEA 1 is a conserved alpha-helical peripheral membrane protein flanked by systeine "fingers" and contains a calmodulin-binding IQ motif. *J Biol Chem.* 1995; 270: 13503–11.
42. **Mills I, Jones A, Clague M.** Involvement of the endosomal autoantigen EEA1

in homotypic fusion of early endosomes. *Curr Biol.* 1998; 8: 881–4.

43. **Sahay G, Alakhova YD, Kabanov VA.** Endocytosis of nanomedicines. *J. Con. Rel.* 2010; 145: 182–95.
44. **Lu Y, Low PS.** Folate mediated delivery of macromolecular anticancer therapeutic agents. *Adv Drug Deliv Rev.* 2002; 54: 675–93.
45. **Yu D, Fukuda T, Kuroda S, *et al.*** Engineered bio-nanocapsules, the selective vector for drug delivery system. *IUBMB Life.* 2006; 58: 1–6.
46. **Tuoya, Hirayama K, Nagaoka T, *et al.*** Identification of cell surface marker candidates on SV-T2 cells using DNA microarray on DLC-coated glass. *Biochem Biophys Res Commun.* 2005; 334: 263–8.
47. **Samah AS, Yuh Sugii, Tuoya, *et al.*** Identification of TM9SF2 as a candidate of the cell surface marker common to breast carcinoma cells. *Clin Oncol Cancer Res.* 2009; 6: 1–9.

ARTICLE
Journal of Cellular Biochemistry 112:318–329 (2011)

Journal of Cellular Biochemistry

Extracellular Matrix Modulates Insulin Production During Differentiation of AR42J Cells: Functional Role of Pax6 Transcription Factor

Kohei Hamamoto,[1] Satoko Yamada,[1] Akemi Hara,[1] Tsutomu Kodera,[1,2] Masaharu Seno,[3] and Itaru Kojima[1*]

[1]*Institute for Molecular and Cellular Regulation, Gunma University, Maebashi, Japan*
[2]*Third Department of Internal Medicine, National Defence Medical College, Tokorozawa, Japan*
[3]*Graduate School of Natural Science, Okayama University, Okayama, Japan*

ABSTRACT

Extracellular matrix (ECM) modulates differentiation of pancreatic β-cells during development. However, the mechanism by which ECM proteins modulate differentiation is not totally clear. We investigated the effect of ECM proteins on differentiation β-cells in vitro. We investigated the effect of basement membrane ECM on differentiation of AR42J cells and rat ductal cells. First, we examined the effect of reconstituted basement membrane, Matrigel on differentiation of AR42J cells induced by activin and betacellulin. Matrigel augmented insulin production and increased the expression of GLUT2, SUR1, and glucokinase. Among various transcription factors investigated, Matrigel markedly upregulated the expression of Pax6. When Pax6 was overexpressed in cells treated with activin and betacellulin, the expression of insulin was upregulated. Conversely, knockdown of Pax6 significantly reduced the insulin expression in cells cultured on Matrigel. The effects of Matrigel on insulin-production and induction of Pax6 were reproduced partially by laminin-1, a major component of Matrigel, and inhibited by anti-integrin-β1 antibody. Matrigel also enhanced the activation of p38 mitogen-activated kinase induced by activin and betacellulin, which was inhibited by anti-β1 antibody. Finally, the effect of Matrigel on differentiation was reproduced in rat cultured ductal cells, and Matrigel also increased the expression of Pax6. These results indicate that basement membrane ECM augments differentiation of pancreatic progenitor cells to insulin-secreting cells by upregulating the expression of Pax6. J. Cell. Biochem. 112: 318–329, 2011.

KEY WORDS: DIFFERENTIATION; β-CELL; MATRIX; PAX6; ACTIVIN A; BETACELLULIN

Differentiation of pancreatic β-cell is strictly controlled by an integrated network of transcription factors. Homeobox transcription factors are important in regulating differentiation [Jonsson et al., 1994; Harrison et al., 1995; Offield et al., 1996; Ahlgren et al., 1997; Naya et al., 1997; Sosa-Pineda et al., 1997; Sussel et al., 1998; Li et al., 1999; Sander et al., 2000; Olbrot et al., 2002; Artner et al., 2007]. Among them, importance of the paired homeobox family is also demonstrated. Pax4-deficient mice lack differentiated β-and δ-cells, and fail to develop mature islets [Sosa-Pineda et al., 1997]. Severe reduction of all endocrine cell types and disruption of the islet architecture are observed in mice lacking Pax6 [Sander et al., 1997; St-Onge et al., 1997]. These transcription factors do not only regulate development but also act to maintain mature β-cell functions [Murtaugh, 2006]. Determination of the factors and molecular signals that regulate these transcription factors is essential not only for understanding the mechanism of pancreatic development but also for establishing the cell based therapy for diabetes.

The importance of extracellular matrix (ECM) in regulating adhesion, migration, proliferation, differentiation and maintenance of mature cell function is well demonstrated. In the pancreas, roles of the basement membrane and its components for islet development and β-cell functions are extensively investigated. For instance, in embryo, attachment to the basement membrane of fetal aorta promotes induction of pancreatic progenitor cells from undifferentiated endoderm [Lammert et al., 2001; Yoshitomi and Zaret, 2004]. Recent study using knockout mice with islet specific ablation of vascular endothelial cells shows severe reduction of β-cells, due to the loss of cell attachment to the basement membrane [Nikolova et al., 2006]. Also, laminin-1, one of the major components of the

*Correspondence to: Itaru Kojima, MD, Institute for Molecular & Cellular Regulation, Gunma University, 3-39-15 Showa-machi, Maebashi 371-8512, Japan. E-mail: ikojima@showa.gunma-u.ac.jp
Received 14 June 2010; Accepted 13 October 2010 • DOI 10.1002/jcb.22930 • © 2010 Wiley-Liss, Inc.
Published online 10 November 2010 in Wiley Online Library (wileyonlinelibrary.com).

basement membrane in fetal pancreas, induces differentiation of early pancreatic cells into insulin-positive cells in mice, whereas collagen type IV which is also an ECM component of the fetal pancreas has been shown to inhibit pancreatic development [Jiang et al., 1999].

In addition to the role of ECM, the importance of integrins are suggested. Integrins are heterodimeric glycoproteins composed of 18 α-subunits noncovalently linked to 8 β-subunits and provide a dynamic interaction of environmental cues and intracellular events by binding to their corresponding ECM [Hynes, 2002]. Of various integrins, the β1 integrin is important for islet development [Jiang et al., 2002; Wang et al., 2005; Yashpal et al., 2008]. Indeed, β1 integrin is broadly expressed in pancreatic epithelium, and in mice lacking β1 integrin, islet structure is disrupted [Kren et al., 2007].

In general, signals from ECM or integrin receptors control cell differentiation by altering the expression of transcriptional factors [Riquelme et al., 2001; Suzuki et al., 2003]. Therefore, the role of cell–matrix interaction on the regulatory network of transcription factors that control pancreatic development is postulated. However, information as to this link is limited. Yoshitomi and Zaret [2004] showed that attachment to aortic endothelial cells induces the expression of Ptf1a in dorsal pancreatic endoderm. They also showed that contact with the basement membrane was required for maintenance of Pdx1 expression in dorsal pancreas. This study demonstrates that signals from ECM modulate pancreatic development by induction of transcriptional factors, but the precise role of ECM or their receptor integrins in the regulation of transcriptional factors is unclear.

In the present study, we investigated the effect of the cell–matrix interaction on differentiation of pancreatic β-cells, in particular, its effect on regulation of transcription factors. By using AR42J cells, a model cell system to study the processes of endocrine differentiation [Mashima et al., 1996], we found that reconstituted basement membrane Matrigel promotes endocrine differentiation, at least in part, by inducing Pax6. In addition, we also found that some of these effects are dependent on laminin-1 and transmitted by the β1 integrin signaling.

MATERIALS AND METHODS

MATERIALS

Recombinant human activin A was provided by Dr. Y. Eto (Central Research Laboratory, Ajinomoto, Kawasaki, Japan). Recombinant human betacellulin (BTC) was prepared as described previously [Seno et al., 1996].

CELL CULTURE

AR42J cells were cultured in Dulbecco's modified Eagle's medium (DMEM) containing 10% fetal bovine serum (FBS) [Mashima et al., 1996]. Cells were incubated with a combination of activin A and BTC to induce differentiation. To evaluate the effect of anti-β1 integrin blocking antibody, cells were resuspended in DMEM containing 10% FBS and preincubated for 15 min with 10 μg/ml anti-β1 blocking antibody (Ha 2/5, BD Biosciences Japan, Tokyo, Japan) or purified hamster IgM before plating.

Rat pancreatic ductal cells were cultured as described previously [Ogata et al., 2004]. More than 95% of the cells were positive for cytokeratin, and cells positive for immunoreactive insulin were not observed before differentiation.

COATING OF DISHES AND SLIDES

Petri dishes (100 mm in diameter) were coated with 25 $\mu g/cm^2$ growth factor-reduced Matrigel, 5 $\mu g/cm^2$ human fibronectin, 10 $\mu g/cm^2$ laminin, 10 $\mu g/cm^2$ collagen type-IV. All extracellular matrices were purchased from BD Biosciences Japan. For morphological and immunohistochemical analyses, glass coverslips were coated with the same concentrations of matrices. In each experiment, 5% bovine serum albumin (BSA) (Sigma-Aldrich Japan, Tokyo, Japan) in phosphate-buffered saline (PBS) was used as a control.

PREPARATION OF RECOMBINANT ADENOVIRUSES

Recombinant adenovirus expressing Pax6 was prepared using a Virapower™ Adenoviral Gateway Expression kit (Invitrogen Japan, Tokyo, Japan). In brief, coding region of mouse Pax6 was digested from plasmid vector encoding mouse Pax6 (pBAT14-mPax6, kindly provided by Dr. Michel German, UCSF, San Francisco, CA) and cloned into an entry vector pENTR3C. To create expression clones and produce recombinant adenovirus, transfer of the mouse Pax6 cassette into the destination vector containing human CMV promoter (pAd/CMV/V5-DEST, Invitrogen Japan) by LR recombination reaction, linearization of plasmid with Pac I and transfection into Adenovirus expressing siRNA for rat Pax6 was constructed using the following oligonucleotide: 5′-CACCGGGTCTGTACCAACGACAATACGAATATTGTCGTTGGTACAGACCC-3′. This oligonucleotide was inserted in the pENTR/U6 entry vector (Invitrogen Japan). Subsequently, U6/shRNAs cassettes were transferred into the destination vector (pAd/BLOCK-iT-DEST, Invitrogen Japan) by LR recombination. Following linearization of plasmid, transfection into 293 cells was performed.

MORPHOLOGICAL ANALYSIS AND IMMUNOHISTOCHEMISTRY

AR42J cells cultured on BSA or matrix-coated glasses were fixed, treated with 0.1% Triton X-100, and then blocked with Blocking Ace solution (Morinaga, Tokyo, Japan). Primary antibodies used were mouse anti-swain insulin (1:100, Spring Bioscience, Freemont, CA), rabbit anti-rat Pax6 (Covance, Berkeley, CA), and rabbit anti-human glucagon (1:100, Dako, Glostrup, Denmark, CA). Secondary antibodies were as follows: biotinylated anti-mouse IgG and biotinylated anti-rabbit IgG (1:400, Vector Laboratories, Brulingam, CA). The fluorescent signals were detected by avidin-conjugated AlexaFluor488 (Molecular Probes, Inc., Eugene, OR). For double-staining, Alexa Fluor568-conjugated anti-mouse IgG and Alexa568-conjugated anti-rabbit IgG (1:600) were used as secondary antibodies.

RNA ISOLATION AND RT-PCR

Total RNA was isolated using TRIZOL reagent (Invitrogen Japan). Total RNA samples were pretreated with DNase I (Nippon gene, Tokyo, Japan) to remove contamination of genomic DNA. First-strand cDNA was synthesized by the SuperScript™III first strand

synthesis system (Invitrogen Japan). Oligonucleotide-primers and PCR-reaction conditions were as previously mentioned [Zhang et al., 2001], except for rat insulin 1 (5′-TACAATCATAGACCATCAGCAAGC-3′ and 5′-CAGTTGGTAGAGGGAGCAGAT-3′ initial denaturation at 95°C for 5 min followed by 35 cycles of 94°C for 30 s, 60°C for 30 s, 68°C for 30 s), rat insulin 2 (5′-AGCCCTAAGTGAACCAGCTACA-3′ and 5′-TGCCAAGGTCTGAAGGTCAC-3′, initial denaturation at 95°C for 5 min followed by 36 cycles of 94°C for 30 s, 60°C for 30 s, 68°C for 30 s), neurogenin-3 (5′-TTCGCACAGTTCCTTGCTGC-3′ and 5′-CGCAACACTGGATTAGGTCACTC-3′ initial denaturation at 95°C for 5 min followed by 32 cycles of 94°C for 30 s, 60°C for 30 s, 72°C for 30 s), and MafA (5′-GATGAAGTTCGAGGTGAAGA-3′ and 5′-GCTCATCCAGTACAGATCCT-3′ initial denaturation at 95°C for 5 min followed by 35 cycles of 94°C for 30 s, 60°C for 30 s, 72°C for 30 s).

REAL-TIME PCR ANALYSIS

One microliter of the first-strand cDNA obtained as described above was used in a 20-μl reaction mixture including 1× SYBR greenER qPCR SuperMix (Invitrogen Japan) and 150 nM primer for rat insulin 2 primer, 200 nM primer for rat Pax6 (5′-CACCGCCCTCACCAACAC-3′ and 5′ GCAGG AGTACGAGGAGGTCTGA-3′), and 200 nM for rat GAPDH (5′-CATGACCACAGTCCATGCCATC-3′; anti-sense, 5′-CACCCTGTTGCTGTAGCCATATTC-3′). The initial cycling conditions involved a hold at 95°C for 10 min, followed by 40 cycles of 94°C for 15 s, then 60°C for 60 s. The signal fluorescence magnitude was detected with an ABI PRISM 7500 Sequence Detector System. Data were normalized to GAPDH signals and presented as mean ± SE.

IMMUNOBLOTTING

Cells were suspended in Laemmli buffer and heated to 100°C for 10 min. After centrifugation, the supernatant was collected, and protein concentration was measured by a BCA protein assay kit (Pierce, Rockford, IL). Cell lysate proteins were separated by 10% sodium dodecyl sulfate polyacrylamide gel electrophoresis, and transferred to polyvinylidene fluoride membrane (Millipore Japan, Tokyo, Japan). The membranes were washed in Tris buffered-saline containing 0.1% Tween-20 and blocked with 5% nonfat dry milk overnight at 4°C. Immunoblotting was performed with the phospho-p42/44 mitogen-activated protein kinase (MAPK), phopho-p38 MAPK, p42/44 MAPK, and p38 detected by chemiluminescence reagents (LumiGLO, Cell Signaling Technology Japan), and the chemiluminescence signals were detected by an image analyzer system (LAS-3000, Fujifilm, Tokyo, Japan).

ELISA FOR INSULIN

Whole cell extracts were obtained by treatment for 24 h on ice in acid–ethanol. The insulin content was determined using Insulin ELISA kit/Rat Ultra Sensitive using rodent insulin standard (Morinaga Biochemicals, Yokohama, Japan), and rat insulinoma INS-1 was used as a positive control. Insulin concentration was normalized with total cellular protein, measured using the BCA protein assay kit (Pierce).

STATISTICAL ANALYSIS

Values are expressed as mean ± SE. The statistical significance was determined using a two-tailed unpaired Student's *t*-test, and differences were considered to be statistically significant when $P < 0.05$.

RESULTS

EFFECT OF RECONSTITUTED BASEMENT MEMBRANE ON DIFFERENTIATION

Previous studies suggested the importance of the basement for pancreatic development [Jiang et al., 1999; Bonner-Weir et al., 2000; Lammert et al., 2001; Yoshitomi and Zaret, 2004; Nikolova et al., 2006]. We first investigated the role of reconstituted basement membrane, Matrigel, on cell differentiation in AR42J cells. We first characterized cell adhesion and morphology in cells cultured on Matrigel-coated or BSA-coated dish (control dish). As shown in Figure 1A-a, naive AR42J cells were round-shaped on the control dish, and time required for majority of the cells to attach to the dish was approximately 12 h. When cells were cultured on Matrigel-coated dishes, cells adhered quite rapidly, and majority of the cells adhered within 30 min (Fig. 1B). When attached, they rapidly flattened and presented spindle-shaped appearances (Fig. 1A-b) which were comparable to those observed in activin-treated cells as previously reported [Ohnishi et al., 1995]. These relatively flattened and spread-shaped appearances were also observed in cells cultured on Matrigel in the presence of BTC and activin (differentiated cells). In differentiated cells cultured on Matrigel, cell size was increased and relatively longer, and multiple processes compared to those cultured on control dish were observed (Fig. 1A-c,A-d). We next measured the expression of mRNA for pancreatic hormones. As previously described [Ohnishi et al., 1995], we confirmed the absence of pancreatic hormones in naive AR42J cell, whereas induction of insulin-2 and pancreatic polypeptide (PP) in differentiated cells (Fig. 1C). Although these expression patterns were unchanged even in cells cultured on Matrigel, we found a remarkable increase in mRNA for insulin-2 in cells cultured on Matrigel. Quantitative RT-PCR analysis demonstrated an approximately sevenfold higher expression of insulin-2 in cells cultured on Matrigel ($P < 0.05$, Fig. 1D). We next performed immunohistochemistry to examine distribution of insulin signals. As shown in Figure 1E, insulin signals were detected in the tips of cell processes in the majority the cells cultured on control dishes. In contrast, cells cultured on Matrigel showed a broadly cytoplasmic distribution of insulin signals. In addition, the signal intensities of insulin in cells cultured on Matrigel were stronger. On the other hand, insulin signals were not detected in naive cells. Consistent with the results obtained by immunohistochemistry, we found approximately twofold increase in insulin content in differentiated cells cultured on Matrigel ($P < 0.05$, Fig. 1F). We further measured the expression of β-cell-associated molecules including GLUT2, glucokinase, SUR1 and Kir6.2, and neuroendocrine markers including PGP9.5, synaptophysin and tyrosine hydroxylase. As reported previously, the expression of GLUT2, SUR1, and glucokinase (Fig. 1G) was induced by the treatment with activin and BTC. In addition, induction of the expression of mRNA for Kir6.2 and tyrosine

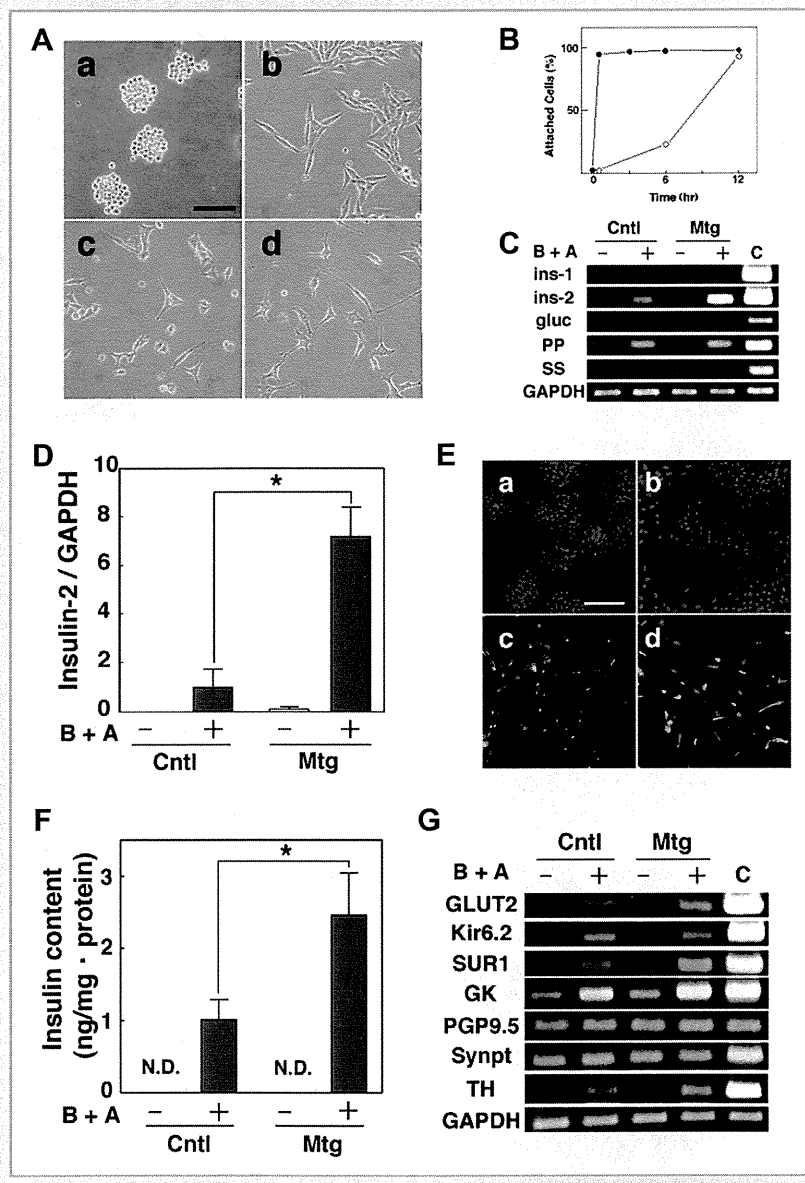

Fig. 1. Effect of reconstituted basement membrane on differentiation of AR42J cells. A: Cell Morphology. AR42J cells (1×10^5 cells/35 mm-dish) were plated on BSA (control matrix) (a,c)-coated and Matrigel (b,d)-coated dishes and incubated for 48 h with (c,d) or without (a,b) 1 nM BTC and 2 nM activin A. Phase contrast micrographs are presented. Bar = 100 μm. B: Time course of effect of matrigel on cell adhesion. Cell were plated on BSA- (○) and matrigel-coated (●) dishes for various periods and the number of attached cells was counted. Values are the mean of three experiments. C: Expression of mRNA for pancreatic hormones. Cells (6×10^5 cells/100 mm-dish) were incubated for 48 h with (+) or without (−) 1 nM BTC and 2 nM activin A (B + A) in control and Matrigel-(Mtg)-coated dishes. The expression of mRNA for insulin-1 (ins-1), insulin-2 (ins 2), glucagon (gluc), pancreatic polypeptide (PP), and somatostatin (SS) was analyzed by RT-PCR. GAPDH serves as a control. mRNA obtained from rat pancreas was used as a positive control (c). Cntl: control, Mtg: Matrigel. D: Quantification of mRNA for insulin-2. Cells were incubated as described in (A), and the expression of mRNA for insulin was quantified by real-time PCR. Results are the mean ± SE for three experiments. $^*P < 0.05$. Cntl: control, Mtg: Matrigel. E: Insulin-staining of differentiated cells. Cells were cultured on control dish (a,c) or Matrigel-coated (b,d) dishes and incubated for 48 h with (c,d) or without (a,b) 2 nM activin A and 1 nM BTC. Staining of insulin by immunofluorescence was obtained. A broad cytoplasmic staining pattern of insulin was observed in differentiated cells cultured on Matrigel (d). Nuclei were stained with 4′, 6-diamidino-2-phenylindole (DAPI). Bar = 100 μm. Cntl: control, Mtg: Matrigel. F: Changes in the insulin content. Cells were treated as described above, and changes in the insulin content and total cellular protein were measured. The normalized values are the mean ± SE for three independent experiments. ND, not detectable. $^*P < 0.05$. Cntl: control, Mtg: Matrigel. G: Changes in the expression of mRNA for islet-associated Molecules. Cells were cultured on control (Cntl) or Matrigel-coated (Mtg) dishes and incubated for 48 h with (+) or without (−) activin A and BTC. mRNA for GLUT2, Kir6.2, SUR1, and glukokinase (GK) were measured by RT-PCR. C: mRNA obtained from INS-1 cells.

hydroxylase was observed. These expression patterns were also observed in cells cultured on Matrigel, but the expression of mRNA for SUR1, glucokinase, and tyrosine hydroxyrase was increased. The expression of mRNA for PGP9.5 and synaptophysin was detected in cells cultured on control dishes and Matrigel, and there were no significant changes during the differentiation. These results suggest that Matrigel promotes differentiation in AR42J cells.

CHANGES IN THE EXPRESSION OF ISLET CELL ASSOCIATED TRANSCRIPTION FACTORS

To determine whether the effect of Matrigel on β-cell differentiation involves changes in the expression of transcriptional factors, we investigated mRNA for islet-associated transcription factors by RT-PCR. As shown in Figure 2A, we found that the expression of Pdx-1, Nkx2.1, Beta2, cdx2/3, cdx4, and lmx1.2 were detected in cells cultured on control dishes and Matrigel, and there were no significant changes during differentiation. The mRNA for Nkx6.1, Isl-1, HB9 and MafA was undetectable before and after differentiation in cells cultured on control dishes and Matrigel. The mRNA for lmx2, lmx1.1, Pax4, Hox1.11, and neurogenin3 was increased during differentiation in cells cultured on control dishes and Matrigel, and there were no significant differences. The mRNA for Pax6 was up-regulated during differentiation in cells cultured on control dishes and Matrigel. However, the expression level was higher in cells cultured on Matrigel. By quantitative RT-PCR, we found an approximately fivefold higher expression of Pax6 in cells cultured on Matrigel (Fig. 2B).

FUNCTIONAL ROLE OF PAX6

The above results indicate that Matrigel induces the expression of Pax6 during differentiation. Previous reports showed that Pax6 promoted transcription of insulin [Sander et al., 1997]. We speculated that Pax6 may be involved in the increase in the insulin expression. To assess the significance of Pax6, we first transfected an adenovirus vector encoding Pax6 into cells cultured on control dishes. To effectively identify transfected cells, we measured immunofluorescence using anti-Pax6 antibody. Some Pax6-transfected cells induced morphological changes, which included relatively longer neurite-like processes (Fig. 3A). In addition, these cells presented relatively intense signals of insulin with broadly cytoplasmic localization. Consistent with results obtained by immunohistochemistry, quantitative RT-PCR analysis demonstrated an approximately fivefold increase in the expression of mRNA for insulin-2 in Pax6-transfected cells ($P < 0.05$, Fig. 3B). However, the expression levels of insulin-2 in Pax6-transfected cells were lower than that of untransfected cells cultured on Matrigel ($P < 0.05$). Effect of combination of Matrigel and Ad-Pax6 was nearly identical to that of Matrigel alone. Furthermore, Pax6-transfected cells expressed glucagon and somatostatin by RT-PCR analysis (data not shown). To further investigate the functional role of Pax6, we also

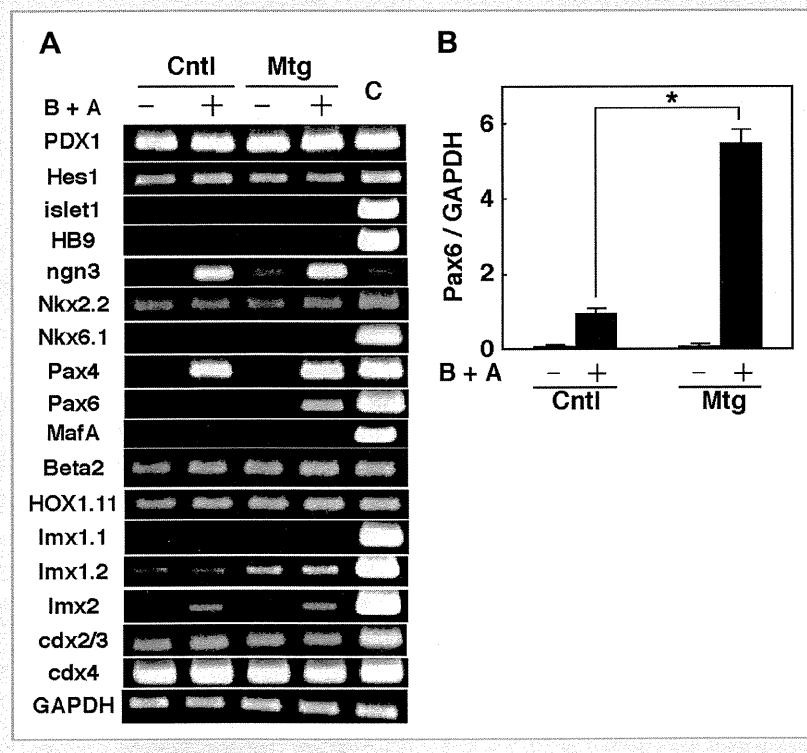

Fig. 2. Effect of matrigel on the expression of mRNA for islet-related transcription factors. A: Changes in mRNA for islet-related transcription factors. Cells were cultured on BSA- (Cntl) or matrigel-coated (Mtg) dishes and incubated for 48 h with (+) or without (−) 1 nM betacellulin and 2 nM activin A (B + A). mRNA from INS-1 cells was used as a positive control (c). B: Quantification of the expression of mRNA for Pax6. Cells were incubated as indicated in (A), and real-time RCR analysis of mRNA for Pax6 was performed. Results are the mean ± SE for four experiments. $^*P < 0.05$.

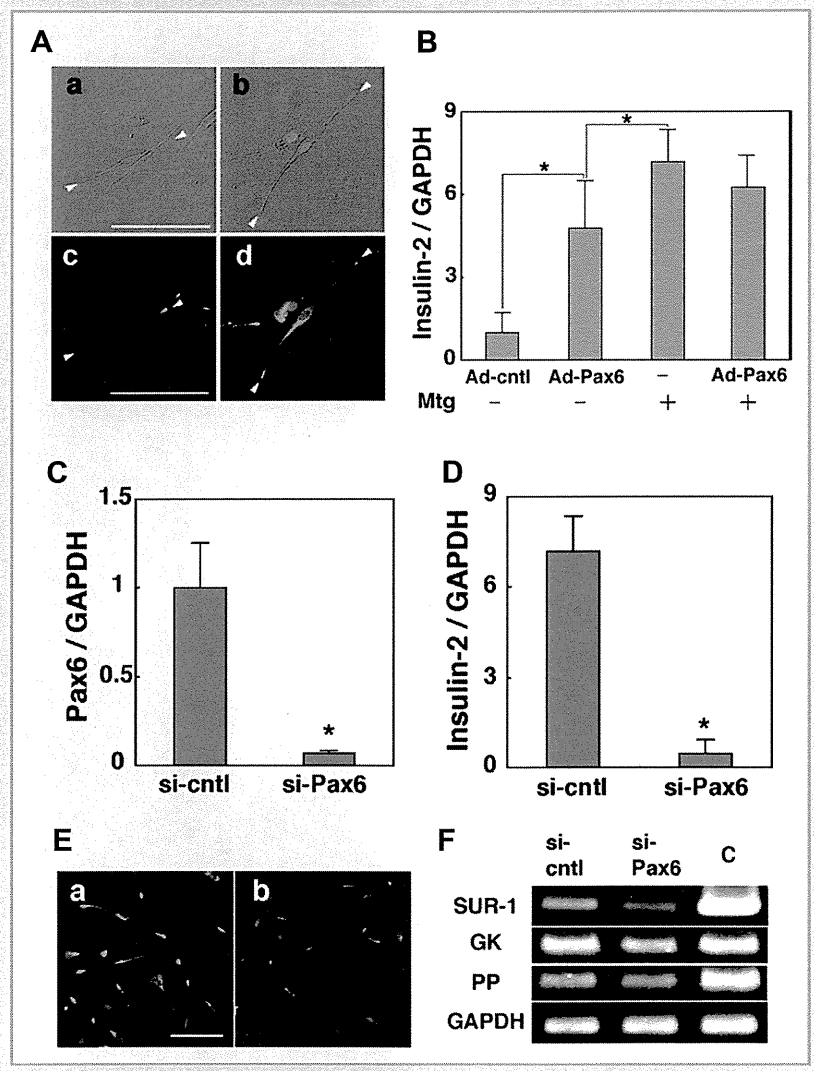

Fig. 3. Effects of overexpression and knockdown of Pax6 on differentiation. A: Morphology of cells overexpressing Pax6. Cells were infected with adenovirus encoding full-length cDNA for mouse Pax6 and incubated for 72 h with 1 nM BTC and 2 nM activin A in BSA-coated dishes. Upper panels (a,b) show morphology of Pax6-transfected cells. Effectively transfected cells were identified by Pax6-specific antibody (red), and the immunostaining of Pax6 was overlaid on Nomarski images (b). Adenovirus encoding lacZ gene was used as control (a). Lower panels (c,d) show overlaid images of Pax6 (red) and insulin (green), which are corresponding images of upper panels. Arrowheads indicated the tip of cell process in a single cell. Bar = 100 μm. B: Effect of overexpression of Pax6 on the expression of mRNA for insulin-2. The expression of mRNA for insulin-2 in Pax6-transfected (Ad-Pax6), LacZ-transfected control (Ad-cntl), non-transfected cells cultured on Matrigel (Mtg) and Pax6-transfected cells cultured on Matrigel was quantified by real-time PCR. Results were normalized to GAPDH. Values are the mean ± SE $^*P < 0.05$. C: Knockdown of pax6 mRNA using siRNA specific to rat Pax6. Cells cultured on matrigel and infected with adenovirus encoding specific siRNA for Pax6 (si-Pax6) and control vectors (si-cntl) were treated with 1 nM BTC and 2 nM activin A. The expression levels of endogenous pax6 mRNA were detected after incubation for 72 h by real-time PCR. Results were normalized to GAPDH and values are the mean ± SE $^*P < 0.05$. D: Effect of knocking down of Pax6 on the expression of mRNA for insulin-2. Cells were treated as in (C), and real-time RCR analysis was performed to quantify the amount of mRNA for insulin-2. Results were normalized to GAPDH and values are the mean ± SE $^*P < 0.05$. E: Effect of siPax on the expression of insulin. Cells transfected with siPax (b) or siLacZ (a) were cultured on Matrigel-coated dishes in the presence of activin A and BTC. Nuclei were stained with DAPI (blue color). Bar = 100 μm. F: Changes in the expression of mRNA for SUR1, glukokinase (GK), and pancreatic polypeptide (PP) in differentiated AR42J cells with or without transfection of si-Pax6.

prepared adenovirus encoding siRNA against Pax6 (Ad-siPax6). Knockdown of Pax6 was significant in Ad-siPax6-transfected cells. The levels of mRNA for Pax6 were reduced to 10% compared to those of the control vector ($P < 0.05$, Fig. 3C). Quantitative RT-PCR analysis showed that silencing of Pax6 significantly reduced the expression of insulin-2 ($P < 0.05$, Fig. 3D). mRNA for insulin-2 in Ad-siPax6-transfected cells was approximately 15% of that of the cells transfected with control vector. Additionally, we found a decrease in insulin immunoreactivities in Ad-siPax6-transfected cells (Fig. 3E). Furthermore, we observed a decrease in mRNA for SUR1 and glucokinase in Ad-siPax6-transfected cells, whereas the expression of mRNA for other hormones including PP, glucagons,

and somatostatin was unchanged (Fig. 3F). Note that we did not observe changes in the expression of other transcription factors (data not shown).

EFFECT OF PURIFIED ECM COMPONENTS ON DIFFERENTIATION

Matrigel contains several basement membrane ECMs including laminin-1, collagen type IV, entactin, fibronectin, and heparin sulfate proteoglycan, and former two are known as major components. To determine which components of the Matrigel regulated differentiation, we examined the effect of laminin-1 and collagen type IV. When the cells were cultured on laminin-1, similar morphological changes as seen in the cells cultured on Matrigel were observed in both undifferentiated (Fig. 4A-c) and differentiated condition (Fig. 4A-g). In addition to morphological changes, we found relatively high levels of mRNA for insulin-2 and Pax6 in differentiated cells cultured on laminin-1 compared to those in cells cultured on plastic dish ($P < 0.05$, Fig. 4B,C) although these effects of laminin-1 were less than those of Matrigel. Furthermore, we also detected relatively high levels and broadly cytoplasmic distributions of insulin immunoreactivities in the cells cultured on laminin-1 (Fig. 4D). On the other hand, obvious morphological changes and upregulation of mRNA for insulin-2 and Pax6 were not observed in the cells cultured on collagen type IV (Fig. 4A-d,A-h,B-D). In addition, we also examined the effect of

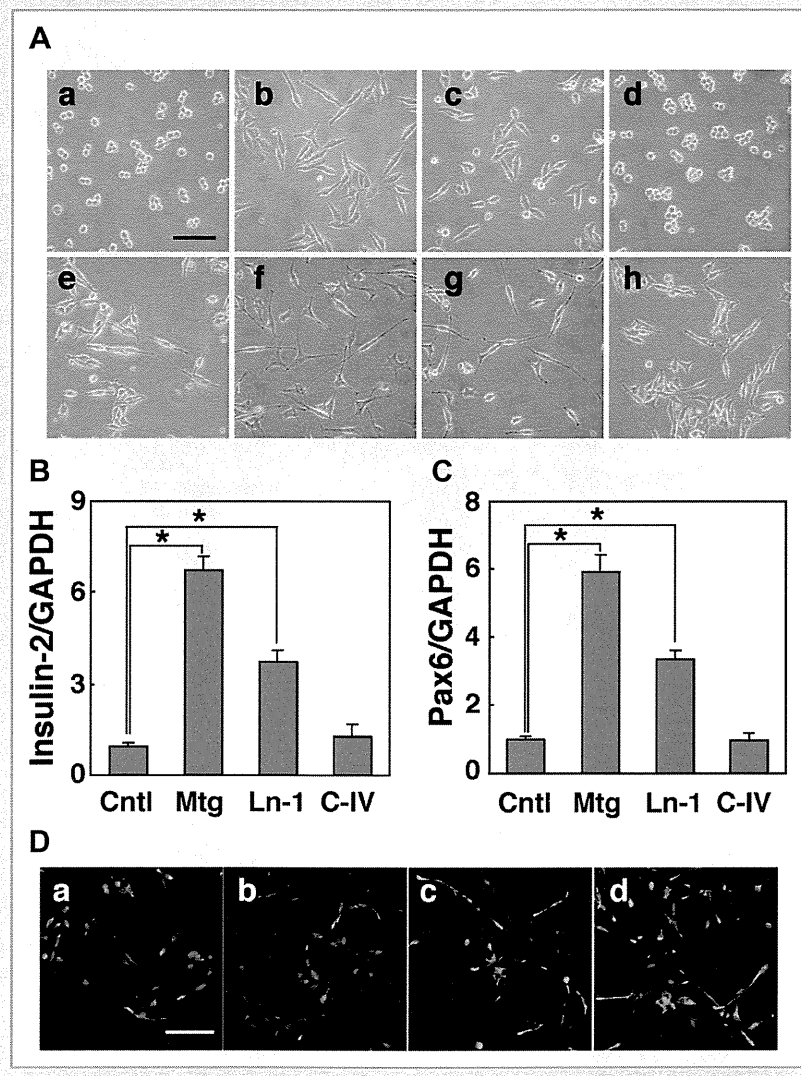

Fig. 4. Effect of purified basement membrane matrix on differentiation. A: Cell morphology. Cells were incubated for 48 h with (e,f,g,h) or without (a,b,c,d) 1 nM BTC and 2 nM activin A on control (a,e), Matrigel-(b,f), laminin-1 (c,g) and collagen type IV (d,h)-coated dishes. Phase-contrast images were presented. Bar = 100 μm. B,C: Quantification of mRNA for insulin-2 and Pax6 in differentiated cells. Cells were incubated for 48 h with 1 nM BTC and 2 nM activin A on control (Cntl), Matrigel (Mtg)-, laminin-1 (Ln-1)- and collagen type IV (C-IV)-coated dishes, and the expression of mRNA for insulin-2 (B) and Pax6 (C) were quantified by real-time PCR. Results are the mean ± SE for three experiments. *$P < 0.05$. D: Insulin-staining of differentiated cells. Cells were cultured as described in (B), and stainings of insulin by immunofluorescence (green) were obtained. A broad cytoplasmic staining pattern of insulin was observed in differentiated cells cultured on Matrigel (d) and laminin-1 (c). a: Control dish. d: Collagen type IV-coated dish. Nuclei were stained with DAPI (blue). Bar = 100 μm.

fibronectin, one of minor component of Matrigel but no obvious changes were observed (data not shown). These data suggest that laminin-1 is the major component of Matrigel responsible for its positive effects on differentiation in AR42J cells although involvement of other signaling molecules in Matrigel is not excluded.

INHIBITORY EFFECT OF ANTI *B*-1 INTEGRIN ANTIBODY ON DIFFERENTIATION

To investigate the molecules that integrate the signals from ECM, we focused on the role of β1-integrin since it is a common integrin receptor isoform corresponding to laminins and is believed to be important for islet cell development [Jiang et al., 2002; Wang et al., 2005; Kren et al., 2007; Yashpal et al., 2008]. As shown in Figure 5A, we found that the expression of β1-integrin was detected in naive cells. Interestingly, the expression of β1-integrin was markedly increased in differentiated cells. The increases in β1-integrin expression in differentiated cells were observed in those cultured on Matrigel, and the expression levels between these cells were not different (data not shown). We then analyzed the effect of anti-β1-integrin antibody on the morphology of the cells cultured on Matrigel. In non-differentiated condition, anti-β1 integrin antibody inhibited morphological changes induced by Matrigel, and cells remained round-shaped (Fig. 5B-b). Cells treated with control antibody were not affected (Fig. 5B-a). In a differentiated condition, cells incubated with anti-β1-integrin antibody were less spread out with shorter processes (Fig. 5B-e,B-f). In contrast, cells cultured on control dish were not affected by anti-β1-integrin antibody in either non-differentiated and differentiated conditions (Fig. 5B-c,B-d,B-g,B-h). These inhibitory effects of anti-β1 integrin antibody were also observed in the cells cultured on laminin-1 (data not shown). By quantitative RT-PCR analysis, we also found a significant reduction of the expression of mRNA for insulin-2 and Pax6 in differentiated cells cultured on Matrigel and laminin-1 with anti-β1-integrin antibody (Fig. 5C,D). Conversely, no remarkable changes in insulin and Pax6 were observed in differentiated cells incubated with anti-β1-integrin antibody when the cells were cultured on control dish. Furthermore, we also confirmed decrease in the insulin signal in differentiated cells cultured on Matrigel treated with anti-β1-integrin (Fig. 5E-a,

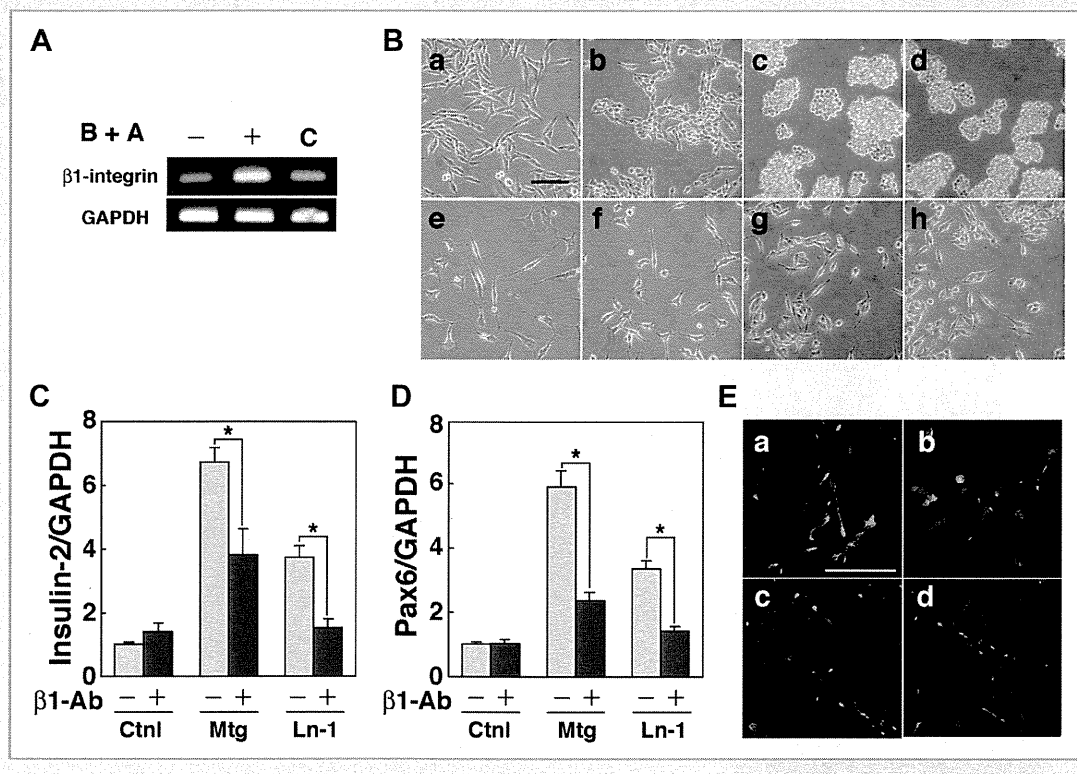

Fig. 5. Effect of anti-β1 integrin antibody on morphological appearance and endocrine differentiation on matrigel and laminin-1. A: Changes in the Expression of mRNA for β1 Integrin. Cells were incubated for 48 h with (+) or without (–) activin A and betacellulin (B + A) on BSA-coated dishes. mRNA for β1 integrin was measured by RT-PCR and mRNA from INS-1 was used as a control (C). B: Effect of Anti-β1 integrin antibody on morphology. Cells cultured on Matrigel (a,b,e,f) or BSA-coated (c,d,g,h) dishes were treated with anti-β1 integrin antibody (b,f,d,h) or control IgM (a,c,e,g). Phase contrast images were obtained 12 h after treatment with (e–h) or without (a–d) activin A and BTC. Bar = 100 μm. C,D: Quantification of mRNA for insulin-2 and Pax6. Cells cultured on Matrigel- (Mtg) and laminin-1 (Ln-1)-coated dishes were incubated for 48 h with activin A and BTC in the presence (+) or absence (–) of anti-β1 integrin antibody (β1-Ab). mRNA for insulin-2 (C) or Pax6 (D) was quantified by real-time PCR. Results were normalized to GAPDH and values are the mean ± SE of three independent experiments. $^*P < 0.05$. E: Immunofluorescence staining of insulin in differentiated cells. Cells were cultured on Matrigel- (a,b) or BSA-coated (c,d) (control) dishes in the presence of anti-β1 integrin antibody (b,d) or control IgM (a,c). They were then incubated with activin A and BTC for 48 h. Immunoreactive insulin is shown in green. Nuclei were stained with DAPI (blue). Bar = 100 μm.